iScience

CellPress
OPEN ACCESS

Review

Toward Tailoring Chemistry of Silica-Based Phase Change Materials for Thermal Energy Storage

Xiao Chen,[1,3,*] Zhaodi Tang,[2,3] Yueqi Chang,[2] Hongyi Gao,[2] Piao Cheng,[1] Zhang Tao,[2] and Junjun Lv[2]

SUMMARY

Efficient thermal energy harvesting using phase change materials (PCMs) has great potential for thermal energy storage and thermal management applications. Benefiting from these merits of pore structure diversity, convenient controllability, and excellent thermophysical stability, SiO_2-based composite PCMs have comparatively shown more promising prospect. In this regard, the microstructure-thermal property correlation of SiO_2-based composite PCMs is still unclear despite the significant achievements in structural design. To enrich the fundamental understanding on the correlations between the microstructure and the thermal properties, we systematically summarize the state-of-the-art advances in SiO_2-based composite PCMs for tuning thermal energy storage from the perspective of tailoring chemistry strategies. In this review, the tailoring chemistry influences of surface functional groups, pore sizes, dopants, single shell, and hybrid shells on the thermal properties of SiO_2-based composite PCMs are systematically summarized and discussed. This review aims to provide in-depth insights into the correlation between structural designs and thermal properties, thus showing better guides on the tailor-made construction of high-performance SiO_2-based composite PCMs. Finally, the current challenges and future recommendations for the tailoring chemistry are also highlighted.

INTRODUCTION

To promote sustainable development and alleviate environmental pollution, large-scale development and utilization of renewable energy has recently received tremendous attentions, such as solar energy, wind energy, biomass energy, hydropower energy, geothermal energy, and tidal energy (Chen et al., 2020c; Neill et al., 2018; Shchukina et al., 2018; Tong et al., 2019; Yuan et al., 2020). However, these energy sources vary with the period of generation. Hence, they are not sufficient to shoulder the responsibility for solving the entire energy needs in the future. As a low-grade energy source, thermal energy is considered as one of the most abundant forms of energy and the basis for many domestic industrial applications. However, the discontinuous supply and awful waste of thermal energy normally reduce the energy utilization efficiency and cause a gap between energy demand and supply in time and space. To improve the thermal energy utilization efficiency and bridge the gap, thermal energy storage techniques (thermochemical energy storage (TCS), sensible heat storage (SHS), and latent heat storage [LHS]) have been extensively explored since the last century (Gao et al., 2018; Huang et al., 2019; Li et al., 2019; Pielichowska and Pielichowski, 2014; Umair et al., 2019; Yang et al., 2019c; Yu et al., 2019).

Among thermal energy storage techniques, TCS has the highest thermal energy density, which is around 5 to 10 times higher than SHS and LHS (Pardo et al., 2014; Shchukina et al., 2018). TCS can be captured through reversible thermochemical reactions. TCS reactions must have a constant conversion efficiency without the reduced energy storage capacity for a long time. Despite the advances and its potential in high-temperature applications, TCS still has long-term stability issue. Therefore, now TCS is primarily tested on a laboratory scale. Conversely, SHS has been developed to an industrial level. SHS refers to heat that can be detected ("sensed") with the change of temperature, which depends on the specific heat capacity of SHS materials. Comparatively, SHS is the easiest and most developed form of thermal storage. However, SHS has the disadvantages of low thermal energy density and thermal energy loss at any temperature. LHS, also known as phase change thermal storage, achieves thermal storage and release during the phase transformation process of phase change materials (PCMs) (Tu et al., 2019; Yang et al., 2019d).

[1]Institute of Advanced Materials, Beijing Normal University, Beijing 100875, PR China

[2]Beijing Advanced Innovation Center for Materials Genome Engineering, Beijing Key Laboratory of Function Materials for Molecule & Structure Construction, School of Materials Science and Engineering, University of Science and Technology Beijing, Beijing 100083, PR China

[3]These authors contributed equally

*Correspondence: xiaochen@bnu.edu.cn

https://doi.org/10.1016/j.isci.2020.101606

Compared with TCS and SHS, LHS based on PCMs is particularly attractive owing to its high thermal energy storage density, nearly constant temperature, and operational simplicity, which can remedy current increasing needs of energy management and energy efficiency (Aftab et al., 2018; Du et al., 2018; Liu et al., 2015; Luan et al., 2016; Yang et al., 2019b). LHS has reached the scale of the pilot plant. In the past century, LHS has been extensively utilized in off-peak electricity storage system, building energy conservation, industrial waste heat recovery, battery thermal management, and smart wearable clothing, etc. (Chen et al., 2018b; Hu, 2020; Huang et al., 2017; Jiang et al., 2018; Lv et al., 2020a, 2020b; Saffari et al., 2018; Saxena et al., 2019; Xiao et al., 2020). According to the chemical compositions, PCMs are divided into organic PCMs, inorganic PCMs, and eutectic PCMs. To date, organic PCMs have been extensively developed in recent years due to large energy storage density, chemical stability, little phase separation, and supercooling degree (Atinafu et al., 2018a, 2018b; Chen et al., 2019a, 2019c, 2019d; Fredi et al., 2017, 2019b, 2018; Li et al., 2018a; Sharma et al., 2015; Tang et al., 2018).

However, pristine PCMs have leakage issue during the solid-liquid phase change process, which seriously hinders their widespread utilization. The best solution is to prepare composite PCMs by packaging PCMs into supporting materials (Chen et al., 2020a; Lin et al., 2018b; Qureshi et al., 2018). To date, the most popular is carbon supporting materials, especially graphene and carbon nanotubes (CNTs) materials (Aftab et al., 2019; Cao et al., 2019; Hu et al., 2020; Qian et al., 2018; Shin et al., 2016; Song et al., 2019; Tang et al., 2019; Wang et al., 2019b; Wu et al., 2019; Xue et al., 2019; Zhang et al., 2019a, 2019b, 2019d; Zhang and Liu, 2019). Undoubtedly, highly thermally conductive carbon materials can accelerate thermal transfer and boost the charging/discharging rates of composite PCMs. In this regard, several reviews have been presented (Chen et al., 2020b; Huang et al., 2019; Ibrahim et al., 2017; Lin et al., 2018b; Tong et al., 2019; Wu et al., 2019; Yang et al., 2019a; Yu et al., 2019). Considering large-scale practical applications of composite PCMs, there are some negative factors in graphene- and CNT-based composite PCMs, such as complex preparation process, low yield, and high cost. These shortcomings have severely hindered their talent display in the fields of practical thermal management. In addition, it is also worth mentioning that composite PCMs may require a low thermal conductivity according to different application scenarios. For instance, PCMs with low thermal conductivity can be used in building architecture, biological thermotherapy, and high technology (like infrared stealth). Ma et al. (2019) prepared the wallboard containing microencapsulated PCMs composed of binary cores and acrylate-based copolymer shells showing excellent thermal insulation performance. Chen et al. (2020a) prepared 3D freestanding flexible CNT sponge-based PCMs with a low thermal conductivity for high-performance thermotherapy of allergic rhinitis. Lyu et al. (2019) prepared nanofibrous Kevlar aerogel-based composite PCMs with a low thermal conductivity for highly efficient infrared stealth.

Benefiting from pore structure diversity, convenient controllability, and excellent thermophysical stability, SiO_2-based composite PCMs have shown greater prospects in practical applications. Pristine SiO_2-based composite PCMs usually have relatively low thermal conductivity, and doping highly thermally conductive additives can improve the thermal conductivity of SiO_2-based composite PCMs. Therefore, SiO_2-based composite PCMs can achieve low or high thermal conductivity. Herein, to guide the tailor-made construction of high-performance SiO_2-based composite PCMs, state-of-the-art advances in SiO_2-based composite PCMs are provided for thermal energy storage from the perspective of tailoring chemistry strategies. In this review, the influences of surface functional groups, pore sizes, dopants, single shell, and hybrid shells on the thermal performances of SiO_2-based composite PCMs (Figure 1) are systematically summarized and discussed, aiming to provide in-depth insights into the relationships between structural designs and thermal properties and a better guide on the construction of high-performance SiO_2-based composite PCMs. Finally, the current challenges and future research directions are also highlighted. This review can contribute a small force to promote the large-scale practical applications of SiO_2-based composite PCMs in the thermal management systems.

CLASSIFICATION AND PACKAGE OF PCMS

Classification of PCMs

PCMs can reversibly utilize latent heat to realize thermal energy storage and release during the phase change process (Li et al., 2018b; Zhang et al., 2019c). PCMs are divided into organic PCMs, inorganic PCMs, and eutectic PCMs according to the chemical compositions (Figure 2) (Wu et al., 2020). Eutectic PCMs are a blend of inorganic and organic PCMs. Compared with inorganic PCMs, organic PCMs have advantages of high LHS density, wide phase transition temperature, no phase separation, little supercooling

Figure 1. Tailoring Chemistry Strategies of Silica-Based Composite PCMs for Thermal Energy Storage

degree, and low density. The working principle of organic PCMs is as follows: when the solid organic PCMs are subjected to heat, they store thermal energy in the form of sensible heat in the initial stage. With the accumulation of heat, the temperature gradually rises until the melting temperature of organic PCMs is reached. At this moment, solid organic PCMs start melting, undergo phase transition process, and thermal energy is stored in the form of latent heat of fusion until the thermal energy is completely stored into PCMs. During phase transition process, the temperature of organic PCMs remains substantially unchanged. With the further accumulation of heat, thermal energy is stored again in the form of sensible heat. The cooling process is similar to the heating process.

Package of PCMs

In practical applications, the leakage issue of pristine PCMs during the solid-liquid phase change process seriously hinders their widespread utilizations. The best solution is to prepare composite PCMs by packaging PCMs into supporting materials. Currently, the two most popular packaging strategies are porous package (shape-stabilized PCMs) (Grosu et al., 2020; Huang et al., 2019; Lu et al., 2019; Shen et al., 2019; Zhang et al., 2020b) and core-shell package (micro/nano-encapsulated PCMs) (Alehosseini and Jafari, 2019; Erdem and Gürbüz, 2019; Kakar et al., 2019; Xia et al., 2020), as shown in Figure 3. In the composite PCMs, PCMs are working substances for thermal energy storage and supporting materials are employed to restrict the flow of liquid PCMs. Generally, the thermal performances of composite PCMs are between those of solid-solid PCMs and solid-liquid PCMs. In general, shape-stabilized PCMs are usually prepared using two-step method: porous supporting materials are first constructed, and then melted PCMs are impregnated into the porous supporting materials via pore-induced capillary force and surface tension (Gao et al., 2018). Micro/nano-encapsulated PCMs are usually prepared using one-step method: PCMs and raw shell materials are simultaneously mixed in a pot to prepare core-shell structural capsules (Jamekhorshid et al., 2014). In this review, SiO_2-based composite PCMs are classified into porous shape-

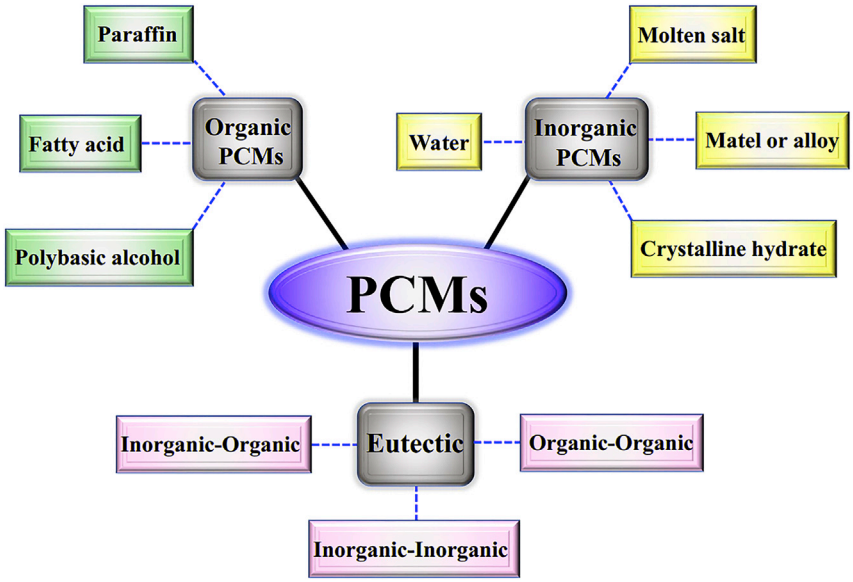

Figure 2. Classification of PCMs Based on Chemical Compositions

stabilized SiO_2-based composite PCMs (referred to as porous SiO_2-based composite PCMs) and micro/nano-encapsulated SiO_2-based composite PCMs.

SILICA-BASED COMPOSITE PCMS FOR THERMAL ENERGY STORAGE

Among numerous composite PCMs, SiO_2 supporting materials have attracted tremendous attention due to their unique pore structure, high adsorption capacity, desirable thermal conductivity, thermochemical stability, non-flammability, ecofriendly nature, and low cost (Li et al., 2013; Zhang et al., 2019e; Zhu et al., 2019). In this review, according to the microstructure of SiO_2, SiO_2-based composite PCMs are divided into two categories: porous SiO_2-based composite PCMs and micro/nano-encapsulated SiO_2-based composite PCMs. In the section on porous SiO_2-based composite PCMs, the influences of functional group types, pore size, and doping additives on the thermal properties of composite PCMs are

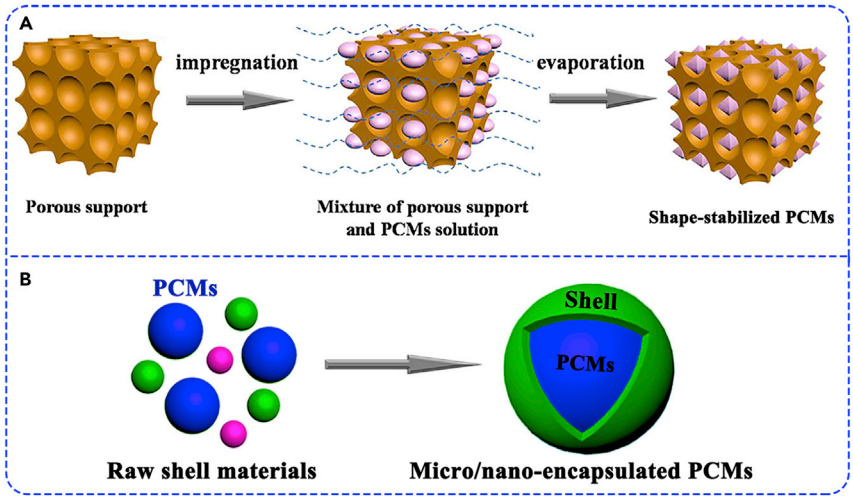

Figure 3. Packaging Strategies of PCMs

(A) Porous package. Adapted with permission from (Gao et al., 2018). Copyright 2018, Elsevier.

(B) Core-shell package. Adapted with permission from (Shen et al., 2019). Copyright 2019, Elsevier.

systematically reviewed. In micro/nano-encapsulated SiO_2-based composite PCMs section, the influences of single shell and hybrid shells on the thermal properties of composite PCMs are systematically reviewed. In general, single SiO_2 shell is unable to satisfy some special functional requirements. In contrast, hybrid SiO_2 shells (including SiO_2-organic shells and SiO_2-inorganic shells) usually harvest the enhanced thermal performances or novel special functions. The corresponding comparison data are summarized in Table 1. These systematic analyses aim to provide profound theoretical and experimental bases for the construction of high-performance SiO_2-based composite PCMs.

Porous Silica-Based Composite PCMs

Mesoporous SiO_2, as a favorable class of supporting materials for the preparation of shape-stabilized composite PCMs, has attracted much attention due to its high specific surface area (Min et al., 2015; Qian et al., 2016), large pore volume (Feng et al., 2011; Kadoono and Ogura, 2014), adjustable pore size distribution (Hu et al., 2009; Johari, 2009), excellent chemical stability (Qian et al., 2015a; Zhang et al., 2013) and strong adsorption ability (Qian et al., 2015a; Wang et al., 2016b). Numerous studies have confirmed that mesoporous SiO_2 has apparent influences on the phase transition behaviors of PCMs, such as latent heat and phase change temperature. This is because the movement of liquid PCMs confined in a narrow nanoporous space of SiO_2 with special functional groups is limited. As a result, the phase change behaviors of the confined PCMs are quite different from the phase change behaviors of PCMs in the free state (Feng et al., 2011; Hu et al., 2009; Zhang et al., 2007). In addition, traditional porous SiO_2-based composite PCMs have relatively low thermal conductivity and poor light-thermal conversion. Herein, the influences of functional group types, pore size, and doped additives on the thermal properties of porous SiO_2-based composite PCMs are systematically analyzed.

Tailoring Chemistry of Functional Groups

In the porous SiO_2-based composite PCMs, functional group types of PCMs and SiO_2 both have significant effects on the phase change behaviors of PCMs. To clarify the phase change mechanisms of different PCMs confined in SiO_2, Liu et al. (2017a) introduced three types of PCMs into mesoporous silica (MS), including octodecane (OCC) with -CH_3, octadecanol (OCO) with –OH, and stearic acid (SA) with -COOH (Figure 4A). Differential scanning calorimetry (DSC) results indicate that there are no endothermic and exothermic peaks in the SA/MS composite PCMs when SA is less than 30 wt %. The same phenomenon also emerges in OCC/MS and OCO/MS composite PCMs when OCC and OCO are less than 30 and 60 wt %, respectively. Namely, the latent heat values are zero during the phase change process. Interestingly, the latent heat starts to appear and gradually increases along with the increase of PCM content when PCMs exceed the limit of the "special mass fraction." However, the latent heat of composite PCMs is much lower than theoretical value. Moreover, the melting temperature decreases, whereas the solidification temperature of composite PCMs increases with the increase of SiO_2. The corresponding mechanisms are as follows: the movement of PCM molecules confined in mesoporous SiO_2 is strongly restricted and the liquid molecules could not crystallize even at a low temperature when the content of PCMs is below the critical level. When the mass fraction of PCMs is higher than the critical level, the crystallization process emerges due to the newly emerging free-moving PCM molecules in SiO_2.

In the porous SiO_2-based composite PCMs, a non-melting interface layer is usually formed between PCMs and SiO_2. This non-melting interface layer severely reduces the available pore volume, thereby reducing the thermal energy storage density of PCMs (Matei et al., 2019). A straightforward method for regulating the thermal performances of porous SiO_2-based composite PCMs is the functionalization of SiO_2 with different functional groups. Matei et al. (2019) studied the functionalization (methyl, phenyl, amino, and carboxylic acid groups) of mesoporous SiO_2 for engineering the non-melting layer and enhancing the thermal energy storage of SA/SiO_2 composite PCMs (Figure 4B). The experimental results (Figure 4C) indicate that methyl and phenyl groups are present inside the non-melting layer, and the non-melting layer volume is similar to the unfunctionalized SiO_2. In contrast, carboxylic acid functionalization markedly reduces the non-melting layer volume because carboxyl groups easily form hydrogen-bonded dimers, thereby obtaining the highest nanoconfined latent heat of 34.5 J/g. This increased nanoconfined latent heat is 15% higher than unfunctionalized SiO_2. As a result, the total latent heat of carboxylic acid-functionalized SiO_2-based composite PCMs is up to 130 J/g. Therefore, the appropriate surface functionalization of SiO_2 can actively suppress the non-melting layer formation and improve the heat storage potential of SiO_2-based composite PCMs.

Supporting Materials	Type of PCMs	Loading Content (wt %)	Melting Point (°C)	Freezing Point (°C)	Melting Enthalpy (J/g)	Decline Ratio of Melting Enthalpy	Freezing Enthalpy (J/g)	Decline Ratio of Freezing Enthalpy	Thermal Conductivity (W/mK)	Ref.
SiO_2	PEG4000	80	57.2	39.0	129.6	15.4%	118.3	13.9%	–	(Min et al., 2015)
SiO_2	PEG6000	66	57.8	43.5	114.8	12.3%	104.6	11.5%	0.61	(Liu et al., 2017b)
SiO_2	Paraffin	45	43.7	38.7	113.3	2.7%	112.0	4.3%	0.13	(Qu et al., 2020)
SiO_2	Myristic acid	65	54.7	46.9	92.0	23.2%	86.0	32.9%	0.37	(Chen et al., 2018a)
SiO_2	Stearic acid	70	71.5	62.4	135.3	16.2%	133.5	15.7%	0.56	(Fan et al., 2017)
SiO_2	$Na_2HPO_4·12H_2O$/ $Na_2SO_4·10H_2O$	70	28.5	–	67.5	–	–	–	–	(Wu and Wang, 2015)
SiO_2	Sodium acetate trihydrate-urea	80	43.5	36.1	164.0	14.7%	–	–	–	(Fu et al., 2019)
SiO_2	Sodium acetate trihydrate-urea	75	43.3	34.6	155.2	13.9%	–	–	–	(Fu et al., 2019)
SiO_2	Sodium acetate trihydrate-urea	70	35.8	31.2	151.6	9.9%	–	–	–	(Fu et al., 2019)
SiO_2	Sodium acetate trihydrate-urea	65	34.4	28.6	136.5	12.7%	–	–	–	(Fu et al., 2019)
Sn^{2+}/SiO_2	PEG6000	66	57.9	44.0	114.7	12.4%	104.1	11.9%	0.77	(Liu et al., 2017b)
$Ag/Sn^{2+}/SiO_2$	PEG6000	66	58.0	44.3	113.9	13.0%	103.8	12.2%	0.84	(Liu et al., 2017b)
Diatomite	Galactitol hexa myristate	52	44.9	44.3	83.8	6.8%	81.1	7.5%	0.19	(Sarı and Biçer, 2012)
Diatomite/Ag	PEG4000	63	59.5	41.0	111.3	2.0%	102.4	1.3%	–	(Qian et al., 2015b)
Diatomite/Ag	PEG4000	63	59.8	39.5	110.7	2.5%	103.3	0.3%	0.82	(Qian et al., 2015b)
SBA-15	Stearic acid	–	69.1	66.7	69.8	–	68.1	–	–	(Kadoono and Ogura, 2014)

Table 1. Summary of SiO_2-Based Composite PCMs for Thermal Energy Storage

(Continued on next page)

Supporting Materials	Type of PCMs	Loading Content (wt %)	Melting Point (°C)	Freezing Point (°C)	Melting Enthalpy (J/g)	Decline Ratio of Melting Enthalpy	Freezing Enthalpy (J/g)	Decline Ratio of Freezing Enthalpy	Thermal Conductivity (W/mK)	Ref.
MCM-41	Paraffin	50	26.0	20.0	68.0	19.0%	50.0	33.8%	–	(Zhang et al., 2018b)
MCM-41	Paraffin	55	26.5	23.0	80.0	13.4%	71.0	14.5%	–	(Zhang et al., 2018b)
MCM-41	Paraffin	60	25.5	22.0	95.0	5.8%	70.0	22.7%	–	(Zhang et al., 2018b)
HO-MCM-41-OH	PEG2000	60	–	–	0	–	0	–	–	(Wang et al., 2016b)
NH_2-MCM-41-CH_3	PEG2000	60	–	–	79.6	14.4%	70.9	15.6%	–	(Wang et al., 2016b)
MCF	Lauric acid	80	42.4	41.3	110.5	16.8%	110.3	15.6%	–	(Mitran et al., 2015)
MCF	Lauric acid	83	42.3	41.2	123.7	10.2%	118.8	12.4%	–	(Mitran et al., 2015)
MCF	Lauric acid	86	41.9	41.0	123.6	13.4%	120.2	14.5%	–	(Mitran et al., 2015)
SiO_2/TiO_2	Paraffin	40	29.0	–	93.7	0.6%	–	–	–	(Li et al., 2018c)
SiO_2/β-AlN	PEG1000	–	60.9	44.8	137.7	–	117.6	–	0.52	(Wang et al., 2009)
SiO_2/Al_2O_3	PEG6000	–	57.1	42.0	123.8	–	126.4	–	0.44	(Tang et al., 2014b)
SiO_2/melamine	Paraffin	98.8	–	–	179.9	–	169.5	–	0.22	(Shi and Zhou, 2019)
SiO_2/carbon fiber	PEG6000	–	57.5	34.8	142.6	–	154.4	–	0.45	(Liu et al., 2018b)
SiO_2/expanded graphite	*n*-Hexadecane	73	20.3	17.9	147.6	0.1%	145.1	1.7%	–	(Fang et al., 2010)
SiO_2/graphene oxide	Stearic acid	–	68.5	64.4	134.4	–	132.5	–	0.28	(Lin et al., 2019)
SiO_2/polystyrene	*n*-Tetradecane	–	2.1	0.4	83.4	–	79.4	–	0.40	(Fu et al., 2017)

Table 1. *Continued*

(Continued on next page)

Supporting Materials	Type of PCMs	Loading Content (wt %)	Melting Point (°C)	Freezing Point (°C)	Melting Enthalpy (J/g)	Decline Ratio of Melting Enthalpy	Freezing Enthalpy (J/g)	Decline Ratio of Freezing Enthalpy	Thermal Conductivity (W/mK)	Ref.
SiO_2/Fe_3O_4	n-Eicosane	–	37.5	30.8	172.5	–	170.9	–	–	(Qian et al., 2019)
SiO_2/SnO_2	PEG600	52	3.1	2.6	58.8	0%	55.5	0.8%	0.71	(Hussain et al., 2018)
SiO_2/TiC/ polymethyl methacrylate	*n*-Octadecane	–	24.3	14.9	93.0	–	94.2	–	–	(Wang et al., 2018b)

Table 1. Continued

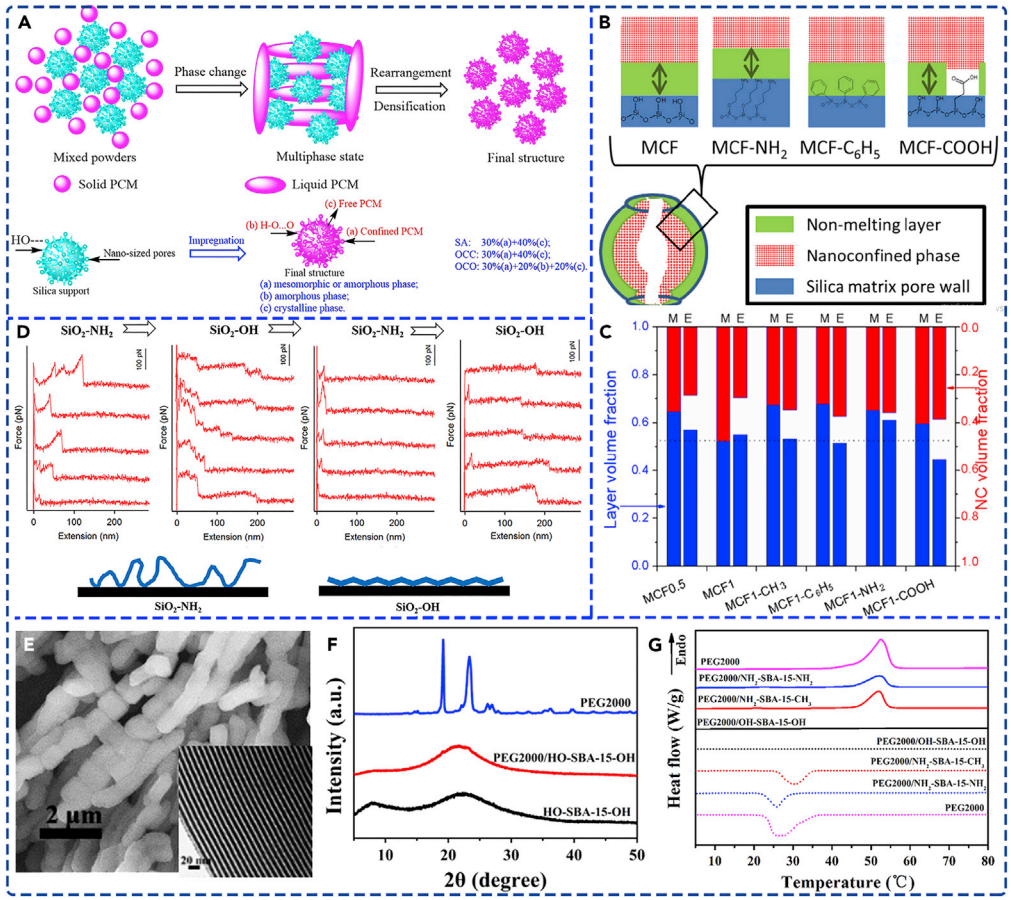

Figure 4. Tailoring Chemistry of Functional Groups

(A) Preparation scheme of various composite PCMs. Adapted with permission from (Qian et al., 2017). Copyright 2017, American Chemical Society.

(B) Schematic representation of mesopores with different functional groups.

(C) Volume fractions for the non-melting layer and nanoconfined phase. Adapted with permission from (Matei et al., 2019). Copyright 2019, Elsevier.

(D) Typical force-extension curves on the surfaces of SiO_2-NH_2, SiO_2-OH, SiO_2-NH_2, and SiO_2-OH.

(E) Scanning electron microscopic (SEM) and transmission electron microscopic (TEM) images of HO-SBA-15-OH.

(F) X-ray diffraction (XRD) patterns.

(G) DSC curves. Adapted with permission from (Wang et al., 2016b). Copyright 2016, Elsevier.

In addition to the small molecular PCMs, polymeric PCMs (such as polyethylene glycol [PEG]) confined in SiO_2 also have a certain volume of non-melting layer or even complete non-melting layer (Wang et al., 2016b). To reduce the non-melting layer volume and arouse the phase transition behaviors of the nanoconfined PEG in the channels of SiO_2, our group (Wang et al., 2016b) functionalized SBA-15 (Santa Barbara Amorphous) with different functional groups (-NH_2 and -CH_3) on the inner and outer surfaces. The results indicate that functional group species on the inner and outer surface of SBA-15 significantly affect the phase transition behaviors of PEG molecules confined in SBA-15 (Figures 4E–4G). Typical force-extension curves indicate that PEG chains exhibit a loop structure in the amino-modified SBA-15, whereas a train structure in the hydroxyl-modified SBA-15 (Figure 4D). These results indicate that the modified methyl groups on the outer surface of SBA-15 are conducive to preventing the leakage of PEG molecules due to the repulsive interaction of the outer methyl groups (Geisler et al., 2010). Therefore, the stronger hydrogen bonds between PEG molecular chains and OH-silicon surface are adverse to the stretching of PEG chains because OH-silicon surface can provide more adsorption sites for PEG molecules than NH_2-silicon surface (Rudner et al., 2005; Wang et al., 2012, 2014a). Moreover, after 50 heating/cooling cycles of PEG/NH_2-SBA-15-CH_3, their phase change temperature and latent heat are also similar to those of the

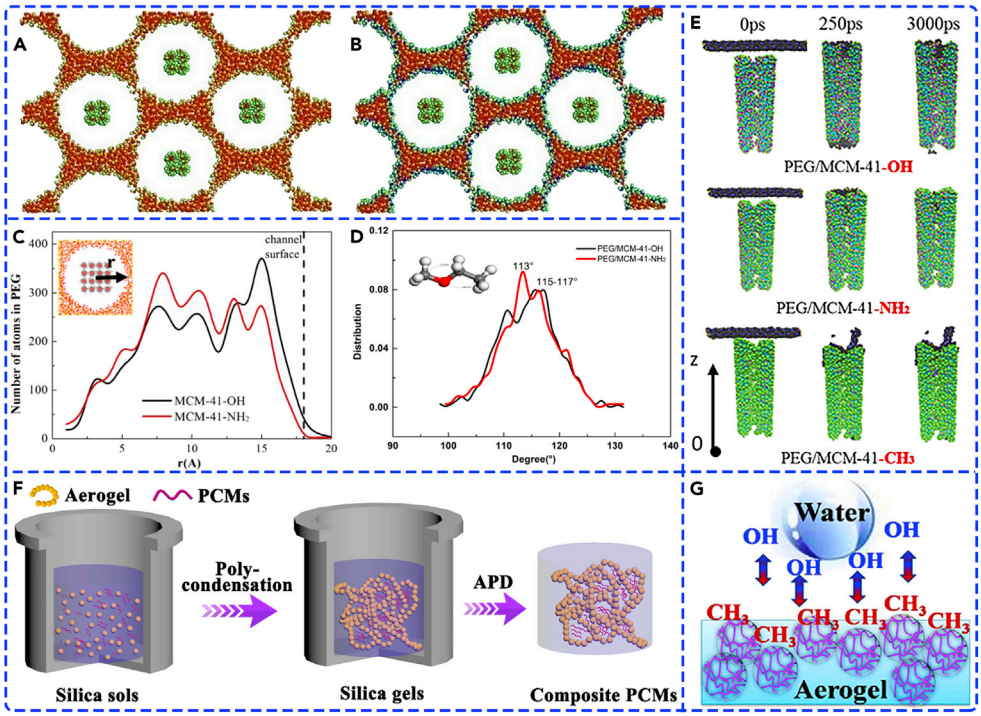

Figure 5. Tailoring Chemistry of Functional Groups

(A) Structural model of MCM-41-OH.

(B) Structural model of MCM-41-NH_2.

(C) Distribution of PEG atoms in MCM-41.

(D) Extension angle of PEG molecules in MCM-41.

(E) Molecular dynamics simulation of PEG molecules in MCM-4. Adapted with permission from (Feng et al., 2020). Copyright 2020, Elsevier.

(F) Preparation scheme of SiO_2 aerogel-based composite PCMs. Adapted with permission from (Li et al., 2020). Copyright 2020, Elsevier.

(G) Schematic of hydrophobic interaction of SiO_2 aerogel. Adapted with permission from (Gao et al., 2019). Copyright 2019, Elsevier.

original composite PCMs, and no obvious leakage of PEG is observed, indicating that the modified NH_2-SBA-15-CH_3 is a good supporting material for PEG stabilization.

Similarly, Feng et al. (2020) also functionalized MCM-41 (Mobil Composition of Matter) with different functional groups (-NH_2 and -OH). Surprisingly, the resultant PEG/MCM-41-OH composite PCMs have no phase transition behavior even at a maximum loading of 70 wt %, while PEG/MCM-41-NH_2 composite PCMs have excellent thermal properties. The latent heat of PEG/MCM-41-NH_2 is 58.76 J/g even at 30 wt % loading. Molecular dynamics simulations (Figures 5A–5E) are used to clarify the mechanism: -NH_2 can reduce the host-guest hydrogen bonding interactions compared with the stronger hydrogen bonding interactions between -OH and PEG molecules. Therefore, amino-functionalized MCM-41 is conducive to the crystallization of PEG molecules. It can be concluded that the interactions between PCMs and mesoporous SiO_2 can be regulated to affect the loading content and phase change behavior of PCMs in mesoporous SiO_2 through surface modification strategy. This surface modification strategy can be extended to other nanopore-based composite PCMs.

Recently, porous SiO_2 aerogel-based composite PCMs have been studied due to the robust mechanical strength, light weight, and adjustable physical and chemical properties (Chen et al., 2019b; Shi et al., 2018; Wu et al., 2018). However, SiO_2 aerogel has a drawback of hydrophilicity, thereby resulting in a poor impregnation of PCMs especially for organic PCMs (Gurav et al., 2010; Sun et al., 2013; Xiangfa et al., 2012). To overcome this disadvantage, Huang et al. (2015) prepared hydrophobic SiO_2 aerogel by replacing Si-OH with Si-CH_3. Based on the hydrophobicity of SiO_2 aerogel, organic hydrophobic PCMs

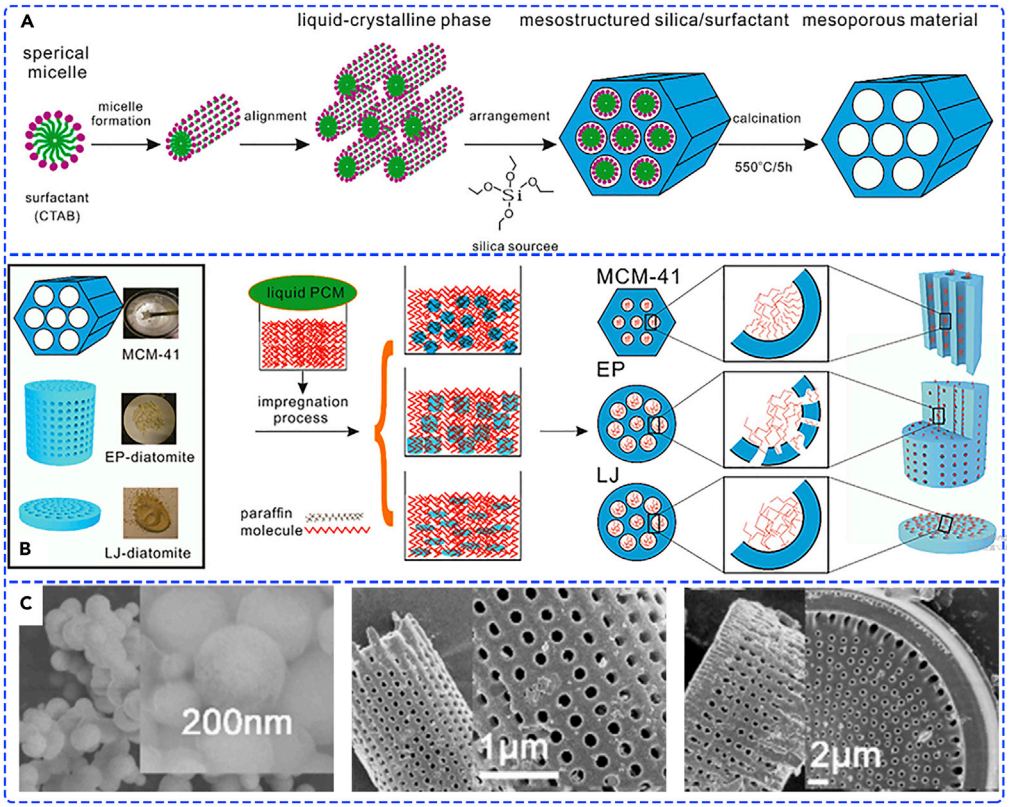

Figure 6. Tailoring Chemistry of Pore Sizes

(A) Preparation scheme of MCM-41.

(B) Preparation scheme of SiO_2-based composite PCMs and schematic orientation of paraffin molecules in SiO_2.

(C) SEM images of MCM-41, EP-diatomite, and LJ-diatomite. Adapted with permission from (Zhang et al., 2018b). Copyright 2018, Elsevier.

(palmitic acid and octadecanol) are infiltrated into SiO_2 aerogel using vacuum infusion. The resultant octadecanol/SiO_2 aerogel composite PCMs have the highest latent heat of 153.71 J/g. Moreover, the hydrophobicity-modified SiO_2 aerogel shows good thermal stability at high temperature. Liu et al. (2020) also prepared hydrophobic monolithic octadecanol/SiO_2 aerogel composite PCMs with high latent heat (127.73 J/g), low thermal conductivity (0.12 W/mK), good hydrophobicity (contact angle of 124°), large compressive strength (11 MPa), and superior thermal cycling stability (Figure 5F). Similarly, Gao et al. (2019) prepared hydrophobic monolithic paraffin/SiO_2 aerogel composite PCMs. During the preparation process, CH_3-rich trimethylmethoxysilane molecules effectively transform SiO_2 clusters from a rigid network structure with high cross-linking degree to a flexible network structure with low cross-linking degree. Such unique SiO_2 cluster not only enhances the flexibility of silicone rubber but also exhibits good hydrophobicity of 140°. The excellent hydrophobicity (140°) is ascribed to the synergistic effect between the surface -CH_3 groups (Figure 5G) and rough surface of SiO_2 aerogel (Nadargi et al., 2009; Yun et al., 2014). The resultant paraffin/SiO_2 aerogel composite PCMs integrate high loading content (70 wt %), large latent heat (122.7 J/g), and outstanding thermal stability (~400°C). These monolithic porous SiO_2 aerogel-based composite PCMs could satisfy large-scope-specific requirements and could be directly utilized in the thermal insulation and thermal protection device due to the synergistic effect between high latent heat and low thermal conductivity of composite PCMs.

Tailoring Chemistry of Pore Sizes

In addition to the surface functional groups, pore sizes have also great influence on the thermal performances of silica-based composite PCMs (Feng et al., 2011; Kadoono and Ogura, 2014). To clarify the corresponding mechanisms, Zhang et al. (2018b) prepared three kinds of SiO_2 supporting materials (MCM-41, EP-diatomite, and LJ-diatomite) with different pore sizes for the encapsulation of paraffin (Figure 6A).

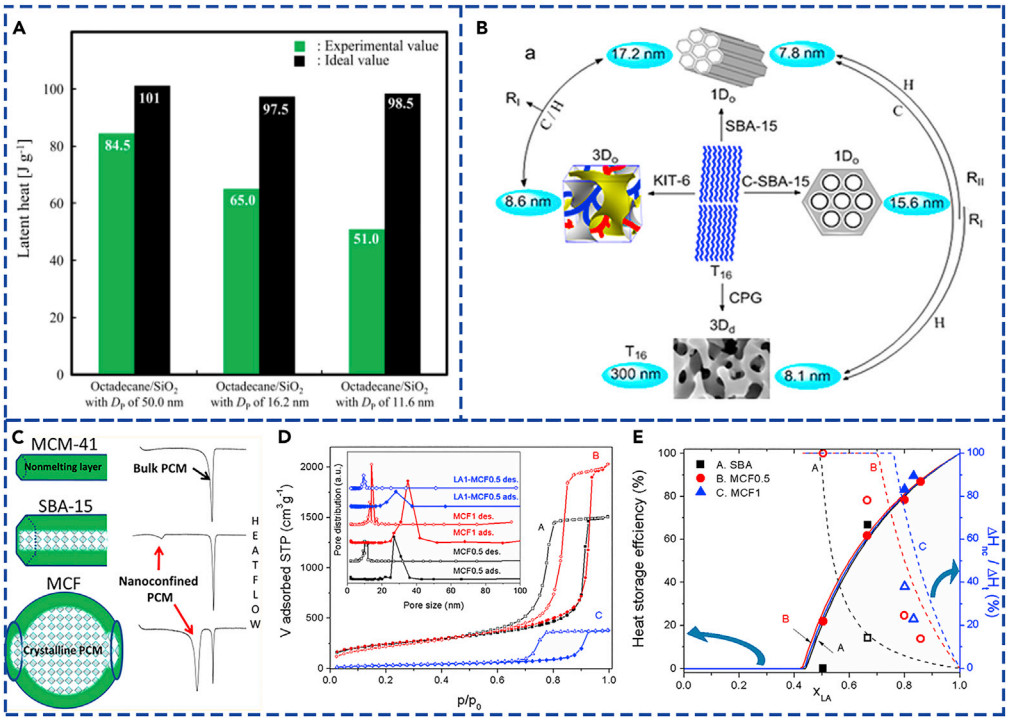

Figure 7. Tailoring Chemistry of Pore Sizes

(A) Latent heat comparison in different pore sizes. Adapted with permission from (Nomura et al., 2015). Copyright 2015, Elsevier.

(B) Scheme of polymorphism of hexadecane in SBA-15, CPG, C-SBA-15, and KIT-6. Adapted with permission from (Wang et al., 2015). Copyright 2015, American Chemical Society.

(C) Scheme of different mesoporous materials (MCM-41, SBA-15, and MCF) and DSC curves.

(D) N_2 adsorption-desorption isotherms for MCF0.5, MCF1, and LA1-MCF0.5.

(E) Thermal performances of SBA-15-, MCF0.5-, and MCF1-based composite PCMs. Adapted with permission from (Mitran et al., 2015). Copyright 2015, American Chemical Society.

MCM-41 has an ordered mesoporous structure with an average pore size of 2.56 nm and a relatively narrow pore size distribution. EP-diatomite has a hierarchical structure with an average pore size of 5.78 nm. LJ-diatomite has a hierarchical structure with an average pore size of 5.65 nm (Figure 6C). After paraffin was infiltrated into different SiO_2 supports, the result SiO_2-based composite PCMs have different thermal properties (Figure 6B). Especially, the free movement of paraffin molecules confined in MCM-41 is strong restricted because the pore size (2.56 nm) of MCM-41 is similar to the length (2.40 nm) of paraffin molecules. The interference of MCM-41 without interconnectivity with the crystallization limits the crystal alignment of paraffin molecules. As a result, the regularities of crystalline regions are reduced and the non-melting layer is increased, thereby reducing the crystallinity of paraffin in MCM-41. In contrast, for EP-diatomite and LJ-diatomite, the natural hierarchical larger pore is rather complex with interconnected and easy-to-access active sites. Therefore, the movement of paraffin molecules in EP-diatomite and LJ-diatomite is relatively free, thereby obtaining a relatively high crystallinity.

Nomura et al. (2015) studied the effect of different pore sizes of SiO_2 on the thermal property of octadecane. The crystallinity and latent heat of the resultant SiO_2/octadecane composite PCMs are increased from 51.6% to 83.6% and from 98.5 J/g to 101 J/g with the increase of the pore size from 11.6 to 50 nm, respectively (Figure 7A). This is due to the formation of a non-melting interface layer in the tiny pore size, thereby reducing the radius of octadecane during the interfacial interactions (Zhang et al., 2018b). In addition, the hydrogen bonding between PCMs and SiO_2 can adjust the strength of the interfacial interactions, and thus affect the phase change behaviors. Wang et al. (2015) also systematically studied the influence of different pore sizes of SiO_2 on the thermal property of hexadecane, including SBA-15 (7.8 and 17.2 nm), controlled porous glass (CPG) (8.1 and 300 nm), carbon-coated SBA-15 (C-SBA-15, 15.6 nm), and KIT-6 (8.6 nm), as shown in Figure 7B. Surprisingly, hexadecane exhibits an only triclinic phase in

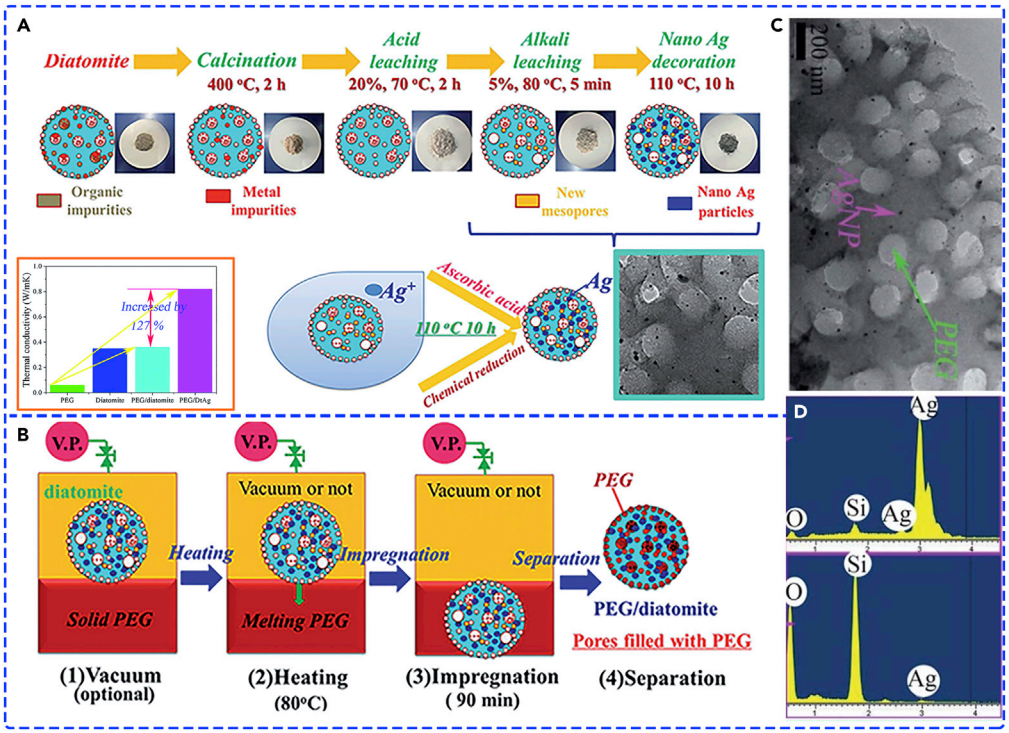

Figure 8. Tailoring Chemistry of Dopants

(A) Preparation scheme of AgNPs-decorated diatomite.

(B) Preparation scheme of composite PCMs.

(C) TEM image of PEG/AgNPs-decorated diatomite composite PCMs.

(D) Energy-dispersive spectrometer (EDS) analysis of AgNPs-decorated diatomite. Adapted with permission from (Qian et al., 2015b). Copyright 2015, Royal Society of Chemistry.

CPG (300 nm), whereas hexadecane exhibits a stable or metastable rotator phase RI or RII in other SiO_2 (7.8–17.2 nm). These results indicate that the stabilization of the rotators is better in smaller pore (<20 nm) or with stronger pore surface interaction due to the substantial involvement of interface energy.

Similarly, Mitran et al. (2015) investigated the effect of different mesoporous SiO_2 (MCM-41 with 2.8 nm, SBA-15 with 6.3 nm, and two disordered mesocellular foams [MCF] with 27–34.9 nm spherical pore connected by 10.4- to 14.9-nm window) on the thermal properties of composite PCMs (Figure 7C). The results indicate that MCF-based composite PCMs have dual temperatures due to two melting or crystallization processes of lauric acid (LA) in the voids and on the external of SiO_2, respectively. To construct theoretical model of nanoconfined LA, the authors measured the specific surface area, pore volume, and pore size distribution of pristine silica. The BET (Brunner-Emmett-Teller) test (Figure 7D) reveals that LA molecules are preferentially adsorbed on the smaller window pore surface. These experimental results are in good agreement with the theoretical results (Figure 7E). DSC results illustrate that two melting peaks at 41.9°C and 31.7°C are detected in LA6-MCF0.5, corresponding the fusion heat of 104.8 and 17.1 J/g, respectively. Similarly, two crystallized peaks at 41.0°C and 14.0°C are detected in LA6-MCF0.5, corresponding to the solidification heat of 105.8 and 17.1 J/g, respectively.

Tailoring Chemistry of Dopants

In general, traditional SiO_2-based composite PCMs have relatively low thermal conductivity (Manoj Kumar et al., 2020). For instance, Ranjbar et al. (2020) prepared n-heptadecane-SiO_2 composite PCMs with a thermal conductivity of 0.28 W/mK for indoor temperature regulation in the buildings. To enhance the thermal conductivity, metal (Qian et al., 2015b), metal oxide (Tang et al., 2014b), and carbon materials (Tang et al., 2014a) are usually introduced into SiO_2-based composite PCMs. For instance, considering the high conductivity of Ag nanoparticles (AgNPs), Qian et al. (2015b) prepared AgNPs-decorated diatomite-based composite PCMs (Figures 8A and 8B). However, the pores of raw diatomite are usually blocked by several

impurities, thereby reducing its porosity. To enlarge its pore size and specific surface area, a facile alkali-leaching method is used in this study. As a result, the large pore size is increased and the micropore size is reduced, thereby enlarging the specific surface area. The pore size distribution shows a similar narrow range of 5–10 nm. The spherical AgNPs with a diameter ranging from 3 to 10 nm are uniformly decorated onto diatomite (Figures 8C and 8D). After PEG is infiltrated into AgNPs-decorated diatomite, the maximum loading content of PEG is 63 wt %, which is 31% higher than that of the raw diatomite. The latent heat of PEG/diatomite/Ag is as high as 111.3 J/g, which is very close to the theoretical value of 113.6 J/g. The thermal conductivity of PEG/diatomite/Ag with 7.2 wt % Ag is 0.82 W/mK, which is 127% higher than that of PEG/diatomite (Figure 8A). Moreover, the supercooling degree of PEG/diatomite/Ag is reduced by 16.3% compared with pristine PEG due to the doped AgNPs. The composite PCMs also exhibit excellent thermal and chemical stability even after 200 melting/freezing cycles.

Similar to Ag doping for the thermal conductivity enhancement of PEG/SiO_2 composite PCMs, Tang et al. (2012) *in situ* doped Cu into PEG/SiO_2 via *in situ* chemical reduction of the metal salt solution using an ultrasound-assisted sol-gel method (Figure 9A). The latent heat of PEG/SiO_2/Cu composite PCMs with 2.1 wt % Cu is 110 J/g, and the corresponding thermal conductivity is enhanced by 38.1% compared with pristine PEG. To further enhance the thermal conductivity of PEG/SiO_2 composite PCMs, Tang et al. (2014b) *in situ* doped Al_2O_3 into PEG/SiO_2 using an ultrasound-assisted sol-gel method (Figure 9B). The latent heat of PEG/SiO_2/Al_2O_3 composite PCMs with 3.3 wt % Al_2O_3 is 124 J/g, and the corresponding thermal conductivity is enhanced by 46.5% compared with pristine PEG. However, the enhancement effect of thermal conductivity for PEG/SiO_2 using doped Al_2O_3 and Cu is still very limited. To dramatically improve the thermal conductivity of PEG/SiO_2 composite PCMs, Liu et al. (2018b) *in situ* doped carbon fiber (CF) into PEG/SiO_2 through a sol-gel process. As a result, the latent heat of PEG/SiO_2/CF composite PCMs with 3 wt % CF is 142.6 J/g, and the corresponding thermal conductivity is enhanced by 164.7% compared with pristine PEG. Moreover, the thermal stability of PEG/SiO_2/CF composite PCMs is greatly improved to 340°C. Attractively, CF-doped PEG/SiO_2 composite PCMs exhibit high absorbability at almost all UV-visible wavebands. High light absorption endows PEG/SiO_2/CF composite PCMs high light-thermal energy conversion efficiency.

In addition to the enhancement of thermal performances of SiO_2-based composite PCMs, advanced multifunctions also need to be developed. Based on this idea, Tang et al. (2017) *in situ* doped titanium black (Ti_4O_7) into PEG/SiO_2 using acid and alkali catalytic sol-gel method for light-thermal conversion and storage. Similarly, they introduced multiwall carbon nanotubes (MWCNTs) into PEG/SiO_2 using an ultrasound-assisted sol-gel method for light-thermal conversion and storage (Figures 9C and 9D) (Tang et al., 2014a). The thermal conductivity of PEG/SiO_2/MWCNTs is 0.46 W/mK, which is enhanced by 53.1% compared with pristine PEG. Importantly, the doped MWCNTs serve as an effective photon capturer and molecular heater of light-thermal energy conversion. Therefore, the resultant PEG/SiO_2/MWCNTs composite PCMs can realize highly efficient light-thermal energy conversion and storage (91.8%). Huang et al. (2015) carbonized the treated SiO_2 aerogel to get a hydrophobic framework with a blackened surface (Figure 9E). As a result, only the carbonized PCMs-impregnated SiO_2 aerogel exhibits superior light-thermal energy conversion and storage, compared with un-carbonized PCMs-impregnated block and PCMs-impregnated carbon block under the same solar illumination (Figure 9F). This carbonization strategy can significantly improve the thermal energy storage and release response to optimize the solar energy utilization allocation.

In summary, functional group types and pore sizes and doped additives have obvious influences on the thermophysical properties of porous SiO_2-based composite PCMs, such as latent heat, phase change temperature, thermal conductivity, and light-thermal conversion efficiency. The main reason is that the thermal movement behaviors of liquid PCMs molecules confined in the nanoporous space of SiO_2 are different from bulk PCMs in the free state. Therefore, not all porous SiO_2 is suitable for the encapsulation of PCMs. Although porous SiO_2-based composite PCMs have made great progress in the thermal energy storage and thermal conductivity regulation, more efforts are still needed to study how to further improve the comprehensive thermophysical properties of porous SiO_2-based composite PCMs. Regretfully, to date, what kind of porous SiO_2 is more suitable for the encapsulation PCMs is still inconclusive. This big challenge needs to be overcame experimentally and theoretically in the future.

Micro/Nano-encapsulated Silica-Based Composite PCMs

In addition to the aforementioned porous SiO_2 for the encapsulation of PCMs, microencapsulation and nanoencapsulation of PCMs are also considered as important packaging technologies and have been

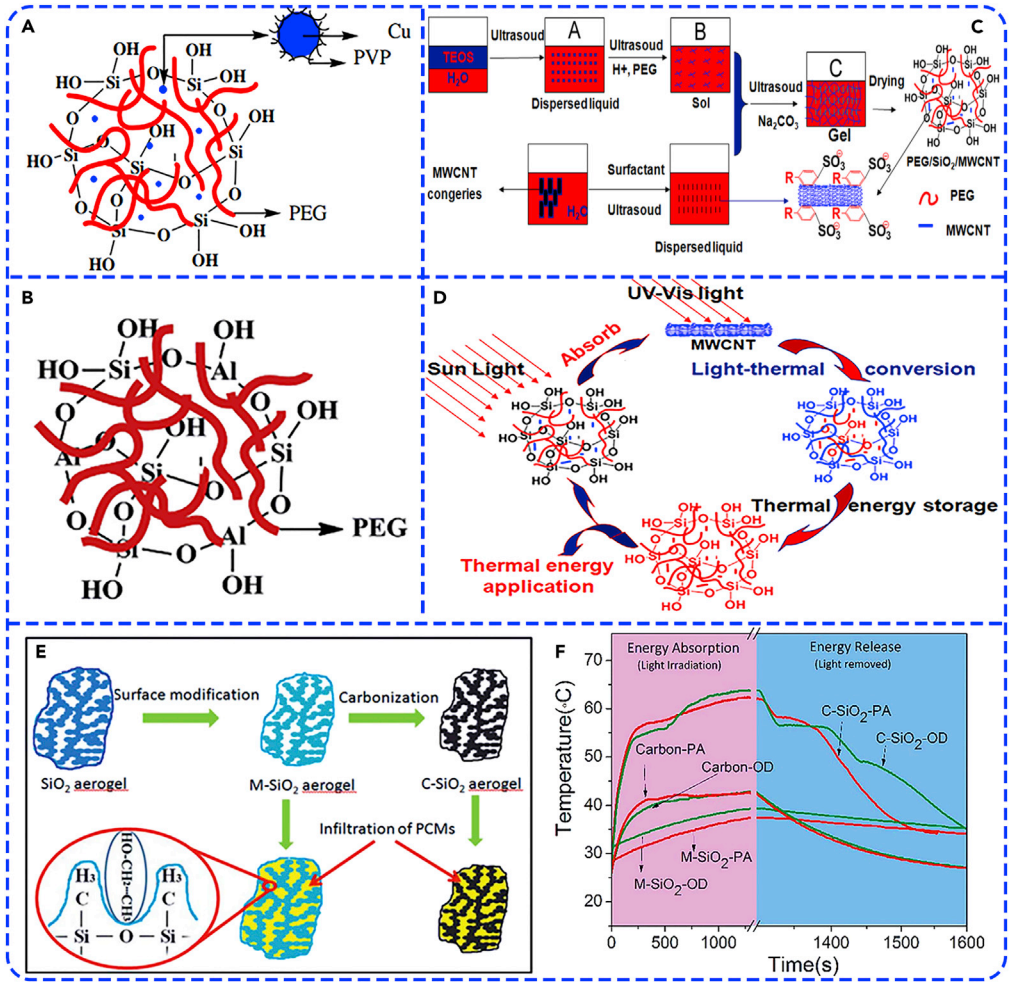

Figure 9. Tailoring Chemistry of Dopants

(A) Doped Cu for thermal conductivity enhancement of PEG/SiO_2. Adapted with permission from (Tang et al., 2012). Copyright 2012, Elsevier.

(B) Doped Al_2O_3 for thermal conductivity enhancement of PEG/SiO_2. Adapted with permission from (Tang et al., 2014b). Copyright 2014, Elsevier.

(C) Doped CNTs for thermal conductivity enhancement of PEG/SiO_2.

(D) Scheme of light-thermal energy conversion and storage. Adapted with permission from (Tang et al., 2014a). Copyright 2014, Elsevier.

(E) Scheme of the hydrophilic-to-hydrophobic surface modification and carbonization process.

(F) Temperature-time curves of PCMs-impregnated compact block, carbonized PCMs-impregnated compact block, and PCMs-impregnated carbon compact block. Adapted with permission from (Huang et al., 2015). Copyright 2015, Royal Society of Chemistry.

well developed in recent years (Jamekhorshid et al., 2014; Zhao and Zhang, 2011). By encapsulating PCMs into hermetically sealed mini containers, the resultant microencapsulated PCMs (MicroPCMs) and nanoencapsulated PCMs (NEPCMs) composed of PCM cores and supporting shells not only can maintain their macroscopic solid form during the solid-liquid phase change processes but also can provide enhanced performances or novel functions (Giro-Paloma et al., 2016). In terms of MicroPCMs and NEPCMs, selecting shell materials is of great importance (Fu et al., 2017; Wang et al., 2016a). According to chemical compositions, the supporting shells are classified into organic shells and inorganic shells. Traditionally, PCMs could be encapsulated into different organic shells through *in situ* polymerization (Su et al., 2006), interfacial polymerization (Cho et al., 2002), and suspension polymerization methods (Taguchi et al., 2007). These organic shells materials mainly include polystyrene (Sánchez et al., 2007), poly(methyl methacrylate)

(Taguchi et al., 2007), melamine formaldehyde resin (Su et al., 2006) and polyuria formaldehyde resin (Brown et al., 2003).

However, MicroPCMs and NEPCMs with organic shells usually have some disadvantages, such as low thermal conductivity, low mechanical strength, serious supercooling, poor thermal and chemical stability, high flammability, and short lifespan (Delgado et al., 2012; Hyun et al., 2014). In this case, the encapsulation of PCMs into inorganic shells is booming. Undoubtedly, inorganic shells usually have much higher thermal conductivity, higher rigidity and mechanical strength, higher thermal and chemical stability, lower supercoiling and flammability, and longer lifespan compared with organic shells (Delgado et al., 2012; Qiu et al., 2015). Comparatively, SiO_2 is one of the most widely used organic shells due to its easy preparation and low cost. Moreover, it can be used for the encapsulation of water-soluble PCMs (Pethurajan et al., 2018; Wu et al., 2014, 2015) and oil-soluble PCMs (Zhu et al., 2015, 2016). The corresponding MicroPCMs and NEPCMs with inorganic SiO_2 shells are usually prepared through *in situ* polymerization or interfacial polycondensation in the sol-gel process (He et al., 2014; Liang et al., 2015; Zhang et al., 2011). However, single SiO_2 shell is usually unable to satisfy some special performance requirements. Therefore, hybrid shells containing SiO_2 shell and organic shells or other inorganic shells with some specific functions are good choices. They usually endure the enhanced performances or novel functions of MicroPCMs and NEPCMs, such as electromagnetic shielding (Jiang et al., 2014), electrochemical energy storage (Xu et al., 2018), and superhydrophobic (Sun et al., 2019), magnetic (Qian et al., 2019), fluorescent (Liu et al., 2018a), photocatalytic (Liu et al., 2018a) and antibacterial functions (Zhang et al., 2016). In this section, SiO_2-based MicroPCMs and NEPCMs with single shell and hybrid shells are systematically reviewed.

Tailoring Chemistry of Single Shell

Unlike inorganic PCMs with serious supercooling issue, organic PCMs generally do not suffer from serious supercooling. However, organic PCMs tend to supercool due to the lack of nuclei when they are encapsulated inside phase change capsules (Zahir et al., 2019). Undoubtedly, high supercooling degree will result in a low thermal response of composite PCMs and hinders their applications in advanced technological fields of precise temperature control. To solve this problem, Liu et al. (2019a) designed nanoencapsulated n-eicosane/SiO_2 using a self-templating strategy (Figure 10). The resultant NEPCMs exhibit superior thermal performances (high thermal storage capability of 99%, high shape stability, and thermal stability). High thermal storage capability indicates that this specific hierarchical nanostructure (internal meso-SiO_2 core and the external SiO_2 shell) can barely inhibit the crystallization of n-eicosane encapsulated in SiO_2. The thermal conductivity of NEPCMs is as high as 1.17 W/mK, whereas pristine n-eicosane has only 0.15 W/mK. This enhanced thermal conductivity is attributed to their internal meso-SiO_2 core and the external SiO_2 shell. This specific hierarchical structure can promote the thermal response and thermal transfer of NEPCMs during the heating and cooling processes. More importantly, the supercooling degree of NEPCMs has only 5.88°C (a decline rate of 24.5%) due to the abundant nucleation sites. This distinct decline rate is much higher than most of the reported microencapsulated n-eicosane (Belessiotis et al., 2018; Geng et al., 2016; He et al., 2015; Li et al., 2015; Liang et al., 2015; Liu et al., 2019b; Ma et al., 2018; Zhang et al., 2015). This unique core-shell structured NEPCMs design strategy provides convincing evidences for effective suppression of the supercooling degree of PCMs.

In addition to nanoencapsulated PCMs, Fredi et al. (2019a) prepared docosane-organosilica microcapsules and studied how the confinements affect the microstructural and thermal properties of the microcapsules. Li et al. (2013) prepared microencapsulated paraffin/SiO_2 through *in situ* emulsion interfacial hydrolysis and polycondensation (Figure 11A). The latent heat of MicroPCMs is only 45.5 J/g. Şahan and Paksoy (2018) prepared microencapsulated SA/SiO_2 using emulsion polymerization, *in situ* emulsion interfacial hydrolysis and polycondensation methods (Figure 11B). Scanning electron microscopic images show that MicroPCMs are uniformly distributed in the poly-methyl methacrylate matrix and maintain their spherical structure. However, the resultant MicroPCMs have only a latent heat of 5.0 J/g with an encapsulation efficiency of 10 wt %. To further enhance the thermal performances of MicroPCMs, Lin et al. (2019) prepared (graphene oxide) GO-modified SiO_2 shell by a sol-gel method and self-assembly process. The thermal conductivity of MicroPCMs is increased by 75% compared with pristine SA. The enhanced thermal conductivity is attributed to the synergistic effect between SiO_2 and GO. In addition, the synergistic effect between SiO_2 and GO can also reduce the supercooling degree of MicroPCMs. In addition to small molecule PCMs, Li et al. (2020) prepared polymer PEG/SiO_2 MicroPCMs (Figures 11C) with a latent heat of 164.9 J/g with a loading fraction of 97 wt %, which is very close to the pristine PEG's value (178.6 J/g).

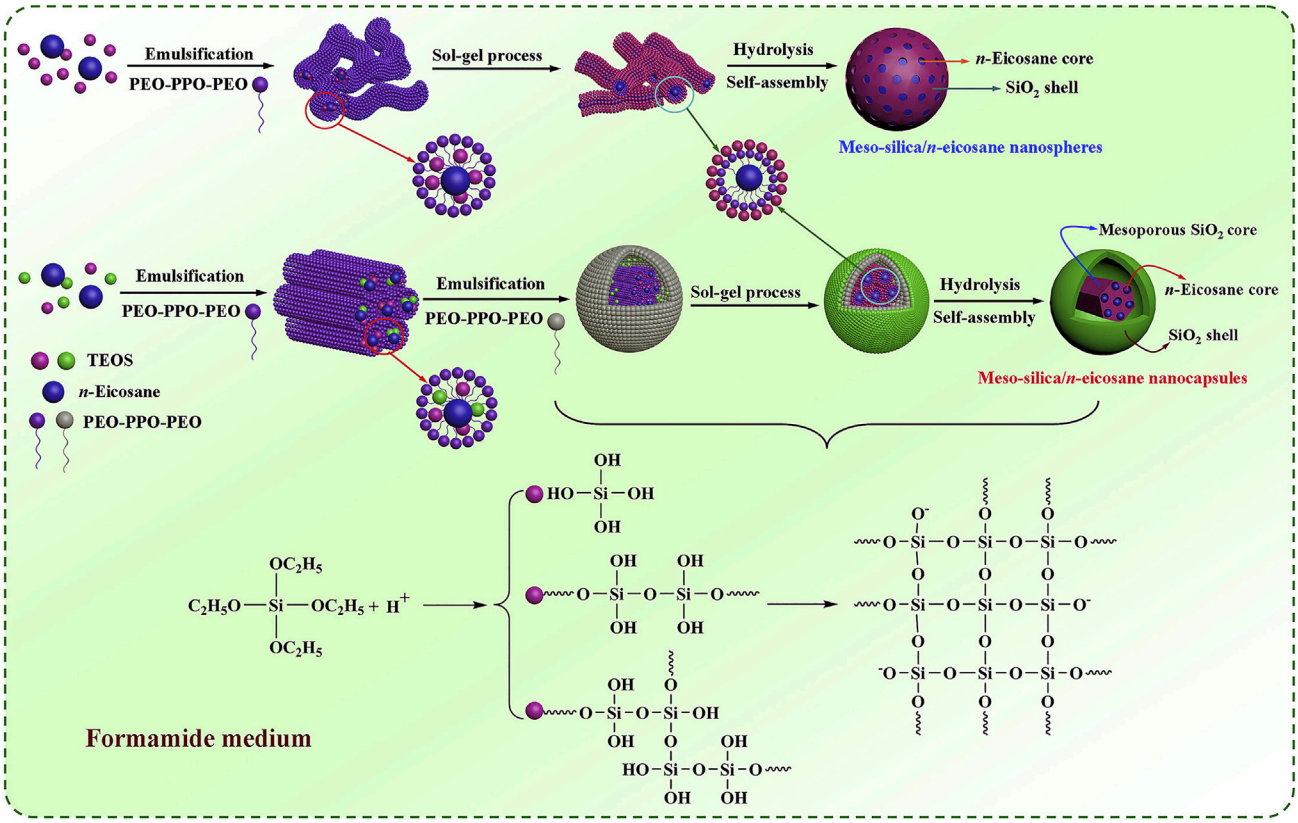

Figure 10. Tailoring Chemistry of Single Shell

Preparation Scheme of n-Eicosane/SiO_2 MicroPCMs. Adapted with permission from (Liu et al., 2019a). Copyright 2019, Elsevier.

Compared with organic PCMs, inorganic hydrated salts have many advantages, such as high thermal energy storage density, non-flammable, non-toxic, and low cost (Lin et al., 2018a; Milian et al., 2017; Mohamed et al., 2017). Liu et al. (2019c) designed sodium phosphate dodecahydrate (DSP)/SiO_2 MicroPCMs through interfacial polymerization and sol-gel method without any extra initiators (Figures 11D). In this MicroPCMs, crystalline $Na_2HPO_4{\cdot}12H_2O$ serves as the core, and tetraethoxysilane (TEOS) and (3-aminopropyl) triethoxysilane (APTES) serve as the SiO_2 precursors (Figures 11E and 11F). Reaction temperature and time would significantly affect the encapsulation efficiency of the MicroPCMs. When the core/shell ratio was 4:1, the resultant MicroPCMs have the highest encapsulation efficiency of 75.3 wt %, the highest melting enthalpy of 177.0 J/g, and the highest thermal conductivity of 0.50 W/mK. It is noteworthy that larger loading content of DSP core and more compact SiO_2 shell would result in a higher thermal conductivity of MicroPCMs because more voids in MicroPCMs are filled with hydrated salts with high thermal conductivity. In addition, the phase change enthalpies of the $Na_2HPO_4{\cdot}12H_2O/SiO_2$ microcapsule after the 30th thermal cycle are still close to that of the microcapsule experiencing the 1st thermal cycle, indicating its good thermal reliability (Figure 11G).

In addition to conventional thermal energy storage function of MicroPCMs or NEPCMs, the introduced diverse inorganic materials with some specified physical or chemical functions can impart advanced other functions to the resultant MicroPCMs or NEPCMs. For instance, the incorporation of magnetic inorganic materials into MicroPCMs or NEPCMs can integrate electromagnetic shielding function. This is because magnetic materials can dissipate electromagnetic energy owing to the eddy current loss and magnetic loss caused by electromagnetic microwaves (Wang et al., 2013, 2014b). Based on this design idea, Jiang et al. (2016) developed dual-functional magnetic MicroPCMs containing PEG/Fe_3O_4 core and SiO_2 shell for the thermal regulating PI (polyimide) films and electromagnetic shielding (Figures 12A–12C). The magnetic MicroPCMs were prepared by reverse-phase interface polycondensation. The resultant magnetic MicroPCMs not only achieve high energy storage efficiency (98%) but also show a superparamagnetic nature. To confirm the electromagnetic shielding function, PI/magnetic MicroPCMs hybrid films with good interfacial adhesion and homogeneity were prepared by casting

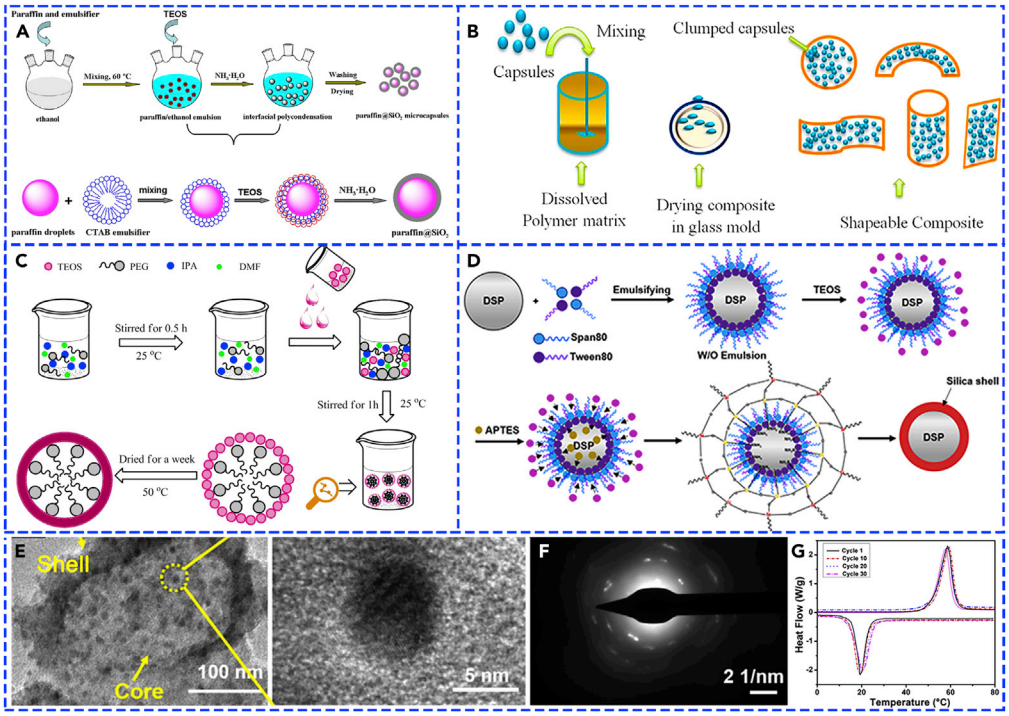

Figure 11. Tailoring Chemistry of Single Shell

(A) Preparation scheme of microencapsulated PCMs. Adapted with permission from (Li et al., 2013). Copyright 2013, American Chemical Society.

(B) Preparation scheme of microencapsulated PCMs. Adapted with permission from (Şahan and Paksoy, 2018). Copyright 2018, Elsevier.

(C) Preparation scheme of microencapsulated PCMs. Adapted with permission from (Li et al., 2020). Copyright 2020, Elsevier.

(D) Preparation scheme of microencapsulated PCMs.

(E) TEM images of microencapsulated PCMs.

(F) Selected area electron diffraction (SAED) pattern of microencapsulated PCMs.

(G) DSC curves of microencapsulated PCMs after 30 heating-cooling cycles. Adapted with permission from (Liu et al., 2019c). Copyright 2019, Elsevier.

the poly(amic acid)/magnetic MicroPCMs mixtures onto glass plates followed by thermal imidization. Thermal gravimetric analyzer (TGA) and differential thermal analysis (DTA) curves indicate that the thermal stability of magnetic MicroPCMs is high enough for the hybrid films to endure the thermal imidization (Figure 12D). Interestingly, the hybrid films show slight magnetic hysteresis in the magnetic hysteresis traces (Figure 12E) compared with magnetic MicroPCMs because polyimide prevents the free rotation of easy magnetization axis of Fe_3O_4 nanoparticles (Sun et al., 2012; Zhang et al., 2015). Moreover, the reflection losses of hybrid films exhibit broadband and frequency-independent characteristics with a minimum absorption of 11.7 dB at 225 MHz and a maximum absorption of 41.2 dB at 1.29 GHz (Figure 12F), indicating that the hybrid films have a high electromagnetic shielding efficiency in the specified frequency bands. Evidently, Fe_3O_4 nanoparticles make a unique contribution to the electromagnetic shielding of the hybrid films. The electromagnetic shielding mechanism of the hybrid films is attributed to the magnetic loss derived from Fe_3O_4 nanoparticles (Bayat et al., 2014). The dual-functional PI-based hybrid films show potential applications for the manufacture of electronic devices with anti-interference and thermal regulation effectiveness.

Tailoring Chemistry of Hybrid Shells

Inorganic-Organic Hybrid Shells. Currently, MicroPCMs and NEPCMs with organic shells have been widely studied due to the excellent sealing tightness and structural flexibility. However, most of organic shells usually release poisonous gas in the application, thus causing environmental and health problems. Moreover, organic shells usually have low mechanical strength, low thermal conductivity, and flammability (Delgado et al., 2012; Hyun et al., 2014). Therefore, some attempts have recently been taken to encapsulate

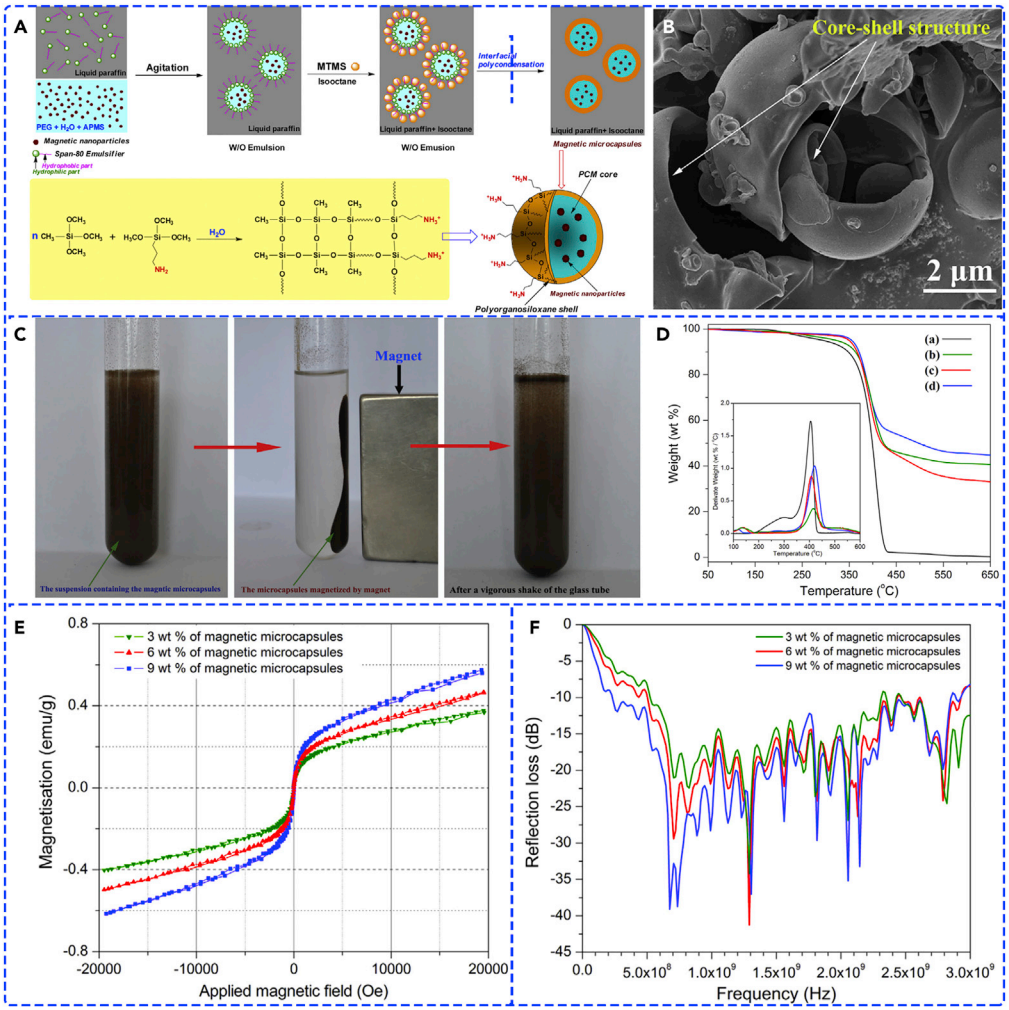

Figure 12. Tailoring Chemistry of Single Shell

(A) Preparation scheme of the magnetic MicroPCMs.

(B) SEM image of the magnetic MicroPCMs.

(C) Digital photographs of the aqueous suspension containing magnetic MicroPCMs before and after application of a magnetic field.

(D) TGA and DTA curves of pure PEG and magnetic MicroPCMs.

(E) Magnetic hysteresis loops of the PI/magnetic MicroPCMs hybrid films.

(F) Reflection loss as a function of test frequency for PI/magnetic MicroPCMs hybrid films. Adapted with permission from (Jiang et al., 2016). Copyright 2016, Elsevier.

PCMs using appropriate inorganic shells because inorganic shell materials have much higher mechanical strength, rigidity, and thermal conductivity compared with organic shell materials (Delgado et al., 2012; Qiu et al., 2015). However, single inorganic shell has some disadvantages, such as poorer endurance and thermal stress (Jiang et al., 2014; Zhang et al., 2015). Therefore, to integrate the advantages of both organic and inorganic shell materials, organic-inorganic hybrid shell is a good solution. For instance, Wang et al. (2018b) prepared MicroPCMs containing n-octadecane core and polymer-SiO_2/TiC hybrid shell via a pickering emulsion polymerization method (Figure 13A). It can be found that hybrid shell has much smaller and more homogeneous size, which is adjustable through altering the particle concentration. The supercooling degree of MicroPCMs can also be effectively reduced by the addition of SiO_2 and TiC nanoparticles, which might be due to the increased thermal conductivity of MicroPCMs (Figure 13B).

To further enhance the thermophysical performances, Fu et al. (2017) prepared one kind of NEPCMs with organic/inorganic hybrid shell via *in situ* miniemulsion polymerization of small droplets and sol-gel reaction

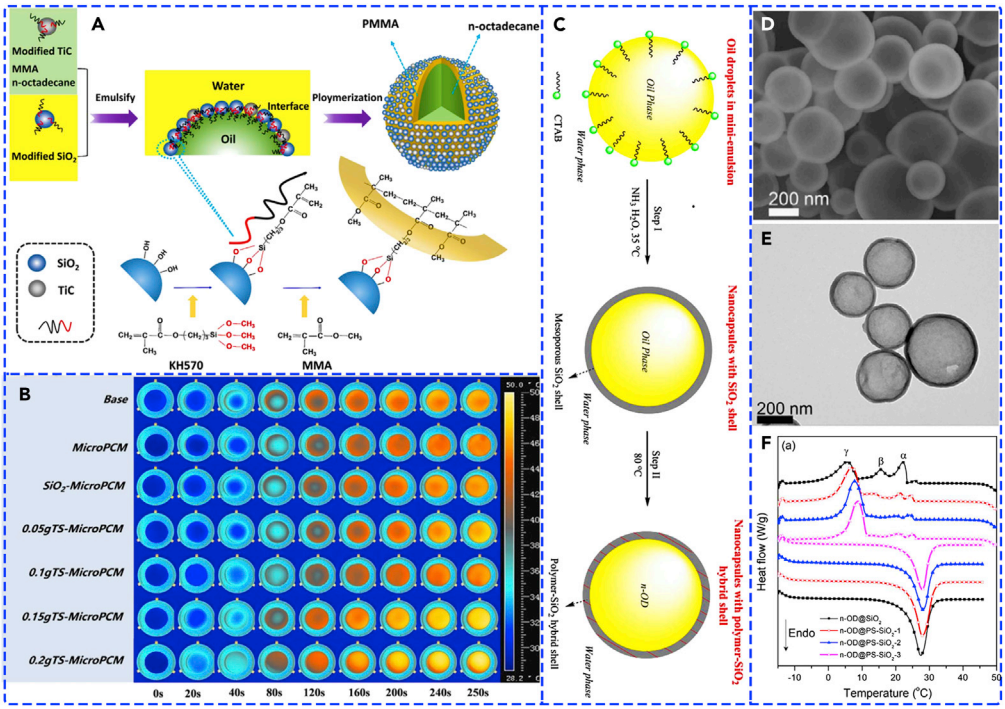

Figure 13. Tailoring Chemistry of Hybrid Shells

(A) Preparation scheme of MicroPCMs with polymer-SiO_2/TiC hybrid shell.

(B) Thermal infrared images of MicroPCMs. Adapted with permission from (Wang et al., 2018b). Copyright 2018, Elsevier.

(C) Preparation scheme of nanoencapsulated n-octadecane with polymer-SiO_2 hybrid shell.

(D) SEM image of nanoencapsulated n-octadecane.

(E) TEM image of nanoencapsulated n-octadecane.

(F) DSC curves of the NEPCMs. Adapted with permission from (Zhu et al., 2018). Copyright 2018, Elsevier.

of tetraethoxysilane. SiO_2 nanoparticles undergo hydrophobic modification. In the NEPCMs, polystyrene (PS) and SiO_2 serve as hybrid shell and n-tetradecane serves as core. The melting temperature and solidification temperature of NEPCMs are 2.13°C and 0.39°C, respectively. The fusion enthalpy and solidification enthalpy of NEPCMs are 83.38 and 79.37 J/g, respectively. These thermal results indicate that the resultant NEPCMs has a high thermal energy storage capacity in the low-temperature environment. It is noteworthy that SiO_2/PS hybrid shell can enhance the thermal stability and thermal conductivity (0.40 W/mK) of NEPCMs because SiO_2 particles are closely deposited on the PS shell. Similarly, Zhu et al. (2018) fabricated NEPCMs containing n-octadecane core and polymer-SiO_2 hybrid shell through interfacial hydrolysis-polycondensation of alkoxy silanes and radical polymerization of vinyl monomers (Figures 13C–13E). The polymer species have large effect on the supercooling degree of NEPCMs (Figure 13F). In addition to the enhanced thermal reliability, the compressive load at yield of NEPCMs is remarkably increased from 14.7 to 65.0 μN due to the particular design of poly(hydroxylethyl methacrylate)-SiO_2 hybrid shell.

Inorganic-Inorganic Hybrid Shells. In addition to organic-inorganic hybrid shell, inorganic-inorganic hybrid shell can also achieve unexpected performance enhancement or new functions. Li et al. (2018c) prepared MicroPCMs containing paraffin core and SiO_2/TiO_2 hybrid shell via a sol-gel method. The thermal conductivity of MicroPCMs is 11.63% higher than that of pristine paraffin. The latent heat of MicroPCMs is only decreased by 6.58% after 1,000 heating/cooling cycles. To further enhance the thermal conductivity, He et al. (2020) prepared NEPCMs containing D-mannitol core and SiO_2/GO hybrid shell via a sol-gel method. The resultant NEPCMs exhibit a high latent heat of 216.7 J/g. The thermal conductivity of NEPCMs is increased by 128.6% compared with pristine D-mannitol. To develop new functions of MicroPCMs, Zhang et al. (2018a) designed MicroPCMs containing paraffin core and SiO_2/Ti_4O_7 hybrid shell via a sol-gel method for light-thermal conversion and storage. The thermal conductivity of MicroPCMs is as high as 1.32 W/mK, which is improved by 334.87% compared with pristine paraffin. More importantly, MicroPCMs with 3 wt % Ti_4O_7 exhibit a high light-thermal conversion efficiency of 85.36% due to the outstanding optical absorption property of Ti_4O_7.

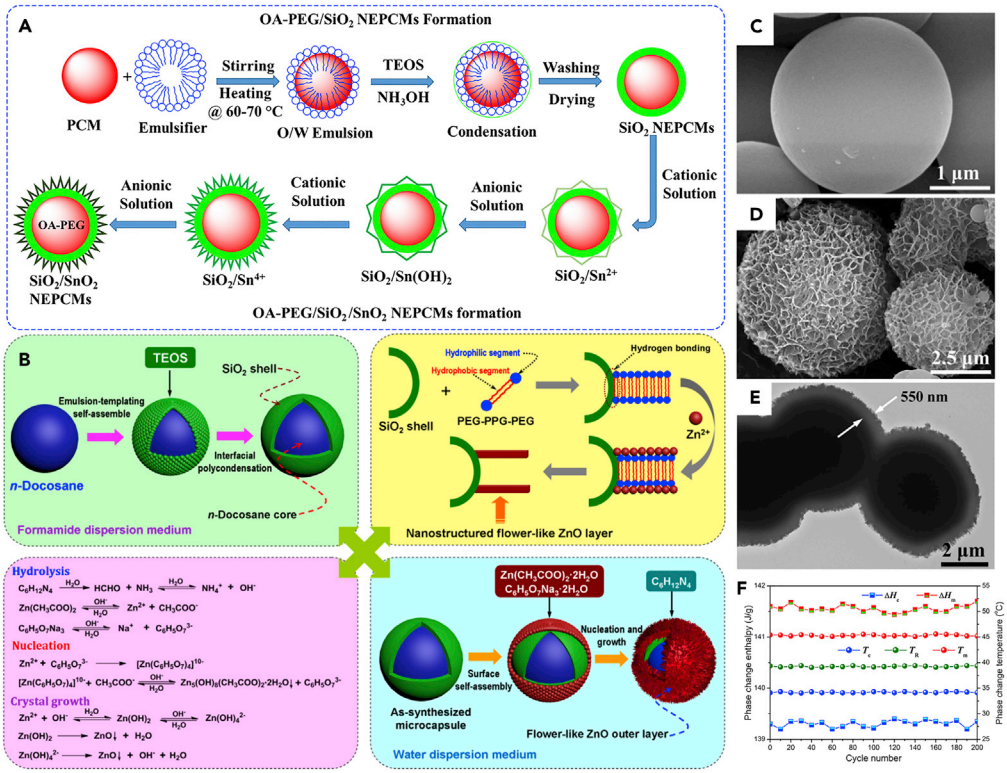

Figure 14. Tailoring Chemistry of Hybrid Shells

(A) Preparation scheme of OA-PEG/SiO_2/SnO_2 NEPCMs. Adapted with permission from (Hussain et al., 2018). Copyright 2018, Elsevier.

(B) Scheme of synthetic route and formation mechanisms of the microencapsulated n-docosane with a ower-like ZnO/SiO_2 hybrid shell.

(C) SEM of as-synthesized microcapsules.

(D) SEM of the microcapsules with a ower-like ZnO/SiO_2 shell.

(E) TEM of the microcapsules with a ower-like ZnO/SiO_2 shell.

(F) Plots of phase change parameters as a function of heating/cooling cycle number for the microcapsules with a flower-like ZnO/SiO_2 shell. Adapted with permission from (Sun et al., 2019). Copyright 2019, Elsevier.

Xu et al. (2018) developed bifunctional MicroPCMs containing n-docosane core and MnO_2/SiO_2 hybrid shell via interfacial polycondensation and template-directed self-assembly for thermal and electrical energy storage. The nanoflake-like MnO_2 layer was constructed on the surface of SiO_2 shell. The resultant MicroPCMs exhibit a high latent heat of 175 J/g with an encapsulation efficiency of 63 wt %. Importantly, MicroPCMs exhibit a higher specific capacitance (312.2 F/g) than traditional MnO_2/SiO_2 solid particles (Hou et al., 2017; Munaiah et al., 2013; Yang et al., 2013; Zhang et al., 2014) when the operation temperature is higher than 45°C. This enhanced specific capacitance is attributed to the *in situ* thermal management of the n-docosane core. Moreover, MicroPCMs exhibit a superior long-term cycling stability with a high capacitance retention of 94.7% after 1,000 charging/discharging cycles due to the MnO_2 layer. Similarly, Hussain et al., (2018) developed bifunctional NEPCMs containing eutectic oleic acid (OA)-PEG core and SnO_2/SiO_2 hybrid shell via *in situ* emulsion interfacial hydrolysis and polycondensation for thermal and electrical energy storage (Figure 14A). The mild-flower-like SnO_2 layer was uniformly formed on the surface of SiO_2 shell. The resultant NEPCMs exhibit a melting temperature of 3.11°C and a latent heat of 58.79 J/g with an encapsulation efficiency of 52 wt %. The thermal conductivity and electrical conductivity of NEPCMs are 0.71 W/mK and 1.08 × 10^{-7} S/cm, respectively. The yield load and hardness of NEPCMs are 89.7 μN and 4.7 GPa, respectively. Importantly, NEPCMs exhibit a specific capacitance of 59.2 F/g. Therefore, these bifunctional MicroPCMs or NEPCMs are good candidates as electrode materials for supercapacitors and Li-ions battery cells.

In addition to thermal energy storage and electrochemical energy storage, Sun et al. (2019) further developed a novel type of bifunctional MicroPCMs containing n-docosane core and ZnO/SiO_2 hybrid shell

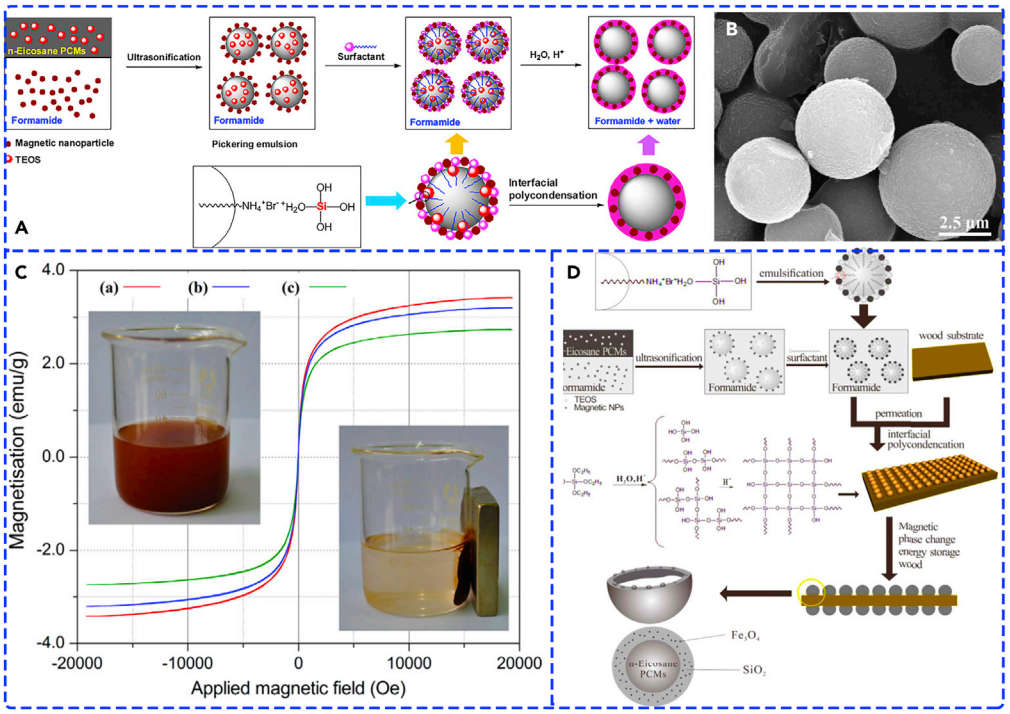

Figure 15. Tailoring Chemistry of Hybrid Shells

(A) Preparation scheme of the magnetic MicroPCMs with n-eicosane core and Fe3O4/SiO2 hybrid shell.

(B) SEM image of the magnetic MicroPCMs.

(C) Magnetic hysteresis loops of the magnetic MicroPCMs. Adapted with permission from (Jiang et al., 2014). Copyright 2014, Elsevier.

(D) Preparation scheme of MicroPCMs with n-eicosane core and Fe_3O_4/SiO_2 hybrid shell on wood surface. Adapted with permission from (Qian et al., 2019). Copyright 2019, Elsevier.

through emulsion-templated interfacial polycondensation for thermal energy storage and superhydrophobic effectiveness (Figure 14B). The flower-like ZnO layer was formed on the surface of SiO_2 shell (Figures 14C–14E). The resultant MicroPCMs exhibit a high latent heat of 139 J/g with an encapsulation efficiency of 79.6 wt %, high phase change reliability, and long-term heating/cooling durability (Figure 14F). Importantly, MicroPCMs exhibit a superhydrophobic surface with a large water contact angle of 159.7° due to the formation of low-surface-energy aliphatic acid coating on the surface of ZnO layer, whereas ZnO layer cannot support superhydrophobicity of MicroPCMs due to large number of hydrophilic hydroxyl groups on the surface of ZnO layer. It is also worth noting that an adaptable aliphatic acid coating is very significant for the superhydrophobic surface of MicroPCMs and that excessive aliphatic acid may reduce the surface hydrophobicity of MicroPCMs. Therefore, these bifunctional MicroPCMs show a great application potential in thermal energy storage, self-cleaning, and antifouling coatings.

Although Fe_3O_4 nanoparticles have excellent magnetic property, they are easily oxidized and tend to aggregate together (Jiang et al., 2014). Considering these issues, Jiang et al. (2014) designed a novel type of bifunctional MicroPCMs containing n-eicosane core and Fe_3O_4/SiO_2 hybrid shell through interfacial polycondensation for thermal energy storage and magnetic effectiveness (Figures 15A and 15B). The SiO_2 shell can effectively protect the magnetic Fe_3O_4 domain from oxidation and aggregation. The resultant MicroPCMs exhibit a high latent heat of 170.2 J/g and high thermal reliability and stability due to the compact Fe_3O_4/SiO_2 hybrid shell. Importantly, MicroPCMs exhibit a superparamagnetism with extremely low magnetic retentivity and coercivity. The magnetization saturation of MicroPCMs is 3.42 emu/g (Figure 15C). This good magnetic performance can make the magnetic MicroPCMs respond quickly to the applied external magnetic field, and thus guarantee that they are subjected to rapid magnetic manipulation in practical applications. Moreover, the supercooling degree of MicroPCMs is suppressed effectively compared with pristine n-eicosane. This is because the nucleation barrier for n-eicosane core is reduced due to the heterogeneous nucleation of inner shell. Similarly, Qian et al., (2019) also designed magnetic MicroPCMs

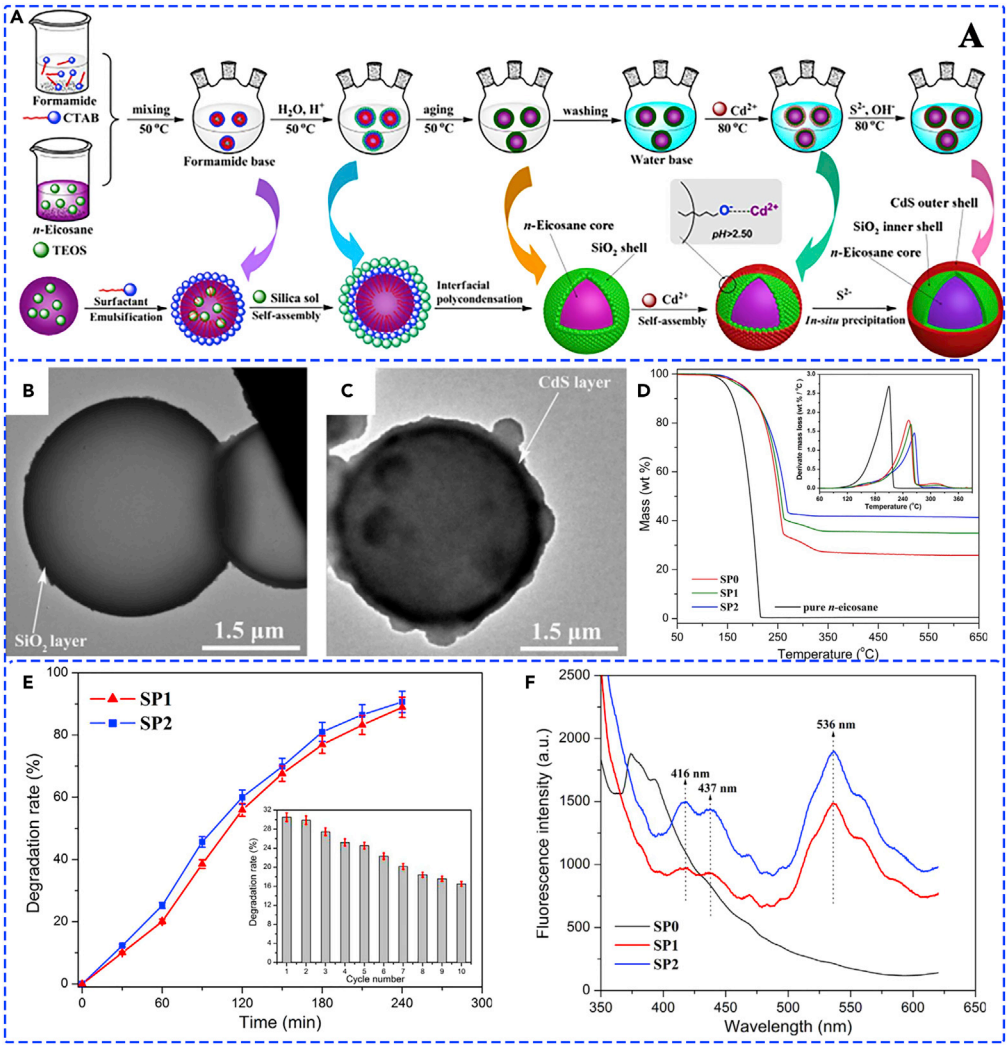

Figure 16. Tailoring Chemistry of Hybrid Shells

(A) Preparation scheme of n-eicosane/SiO_2/CdS MicroPCMs.

(B) TEM image of n-eicosane/SiO_2 MicroPCMs.

(C) TEM image of n-eicosane/SiO_2/CdS MicroPCMs.

(D) TGA and DTA curves of MicroPCMs.

(E) Degradation rate plots of MicroPCMs.

(F) Photoluminescence emission spectra of MicroPCMs. Adapted with permission from (Liu et al., 2018a). Copyright 2018, Elsevier.

containing n-eicosane core and Fe_3O_4/SiO_2 hybrid shell using a sol-gel method (Figure 15D). The resultant magnetic MicroPCMs exhibit a high latent heat of 170.9 J/g and saturation magnetization of 3.70 emu/g. These bifunctional magnetic MicroPCMs can be considered as the intelligent coatings for temperature regulation, anti-radiation, anti-jamming, and electromagnetic-infrared double shielding.

CdS, a semiconductor-type photocatalyst, not only has photocatalytic activity but also has fluorescent feature (Kaur et al., 2019; Ma et al., 2020b; Wang et al., 2019a; Zhen et al., 2018). Considering the dual features of CdS, Liu et al. (2018a) prepared one novel type of MicroPCMs containing n-eicosane core and SiO_2/CdS hybrid shell for solar photocatalysis and fluorescence emission (Figure 16A). First, the inner n-eicosane/SiO_2 was fabricated through the interfacial polycondensation of SiO_2 precursors, in which cetyltrimethylammonium bromide conducted the self-assembly of SiO_2 precursors. Then, the outer CdS layer was constructed on the surface of n-eicosane/SiO_2 MicroPCMs using an *in situ* precipitation method (Chai

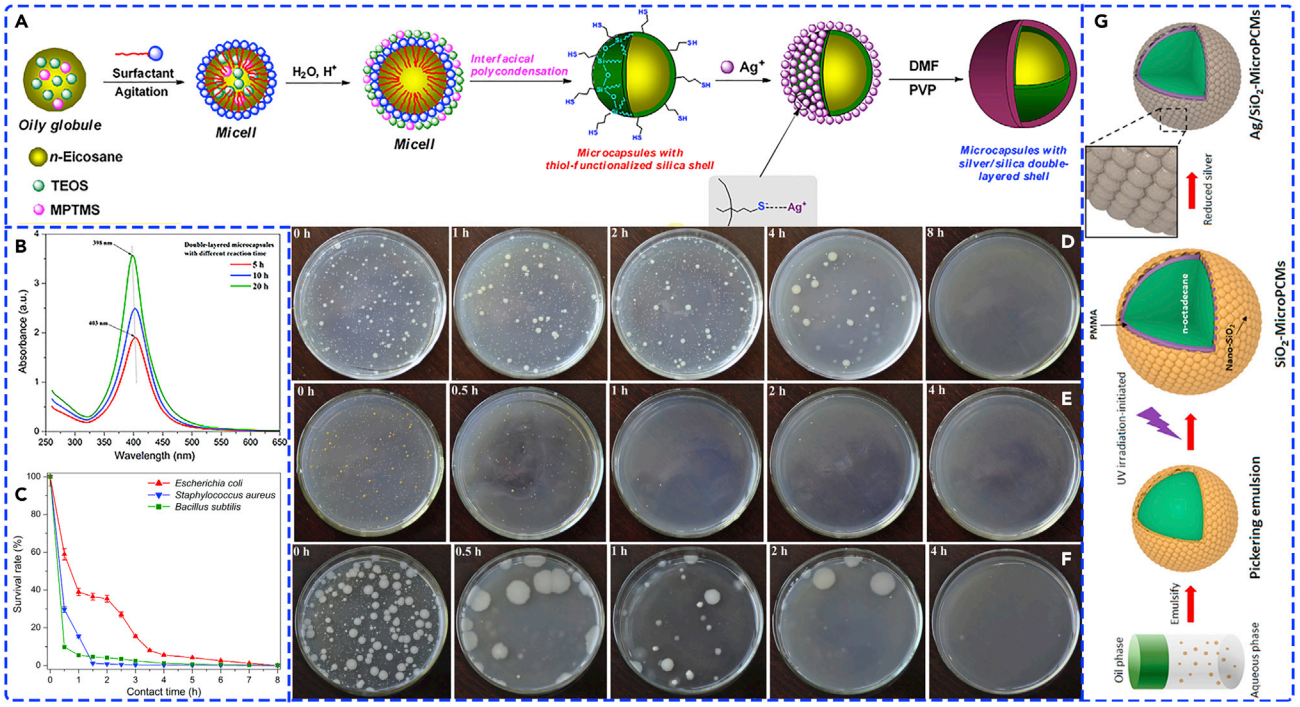

Figure 17. Tailoring Chemistry of Hybrid Shells

(A) Preparation scheme of multifunctional MicroPCMs with n-eicosane core and Ag/SiO_2 hybrid shell.

(B) UV-visible spectra of MicroPCMs at different reaction time.

(C) Plots of the survival rates of different bacteria for MicroPCMs.

(D) Optical photographs of the Petri dishes loading *Escherichia coli* at different contact time.

(E) Optical photographs of the Petri dishes loading *Staphylococcus aureus* at different contact time.

(F) Optical photographs of the Petri dishes loading *Bacillus subtilis* at different contact time. Adapted with permission from (Zhang et al., 2016). Copyright 2016, Elsevier.

(G) Preparation scheme of Ag/SiO_2-MicroPCMs. Adapted with permission from (Wang et al., 2018a). Copyright 2018, Elsevier.

et al., 2015; Kosmulski and Science, 2002). Transmission electron microscopic images (Figures 16B and 16C) clearly exhibit the perfect core-double shell structure of MicroPCMs with a particle size ranging from 2 to 4 μm. TGA and DTA curves (Figure 16D) indicate that the maximum-rate pyrolysis temperatures of n-eicosane/SiO_2 and n-eicosane/SiO_2/CdS microcapsules are both improved due to the encapsulation of rigid inorganic shell. The thermal infrared images indicate that the resultant MicroPCMs have a good thermoregulatory capability. More importantly, CdS is a semiconductor-type photocatalyst and can be activated by visible light. Therefore, the n-eicosane/SiO_2/CdS exhibit a high photocatalytic activity (90%) of methylene blue under the natural sunlight illumination (Figure 16E). It is worth noting that the photocatalytic effectiveness strongly depends on the amount of CdS in the shell (Sudha and Sivakumar, 2015; Xu and Schoonen, 2000). Moreover, the n-eicosane/SiO_2/CdS also exhibit a fluorescent function (Figure 16F) due to the presence of outer CdS layer (Sudha and Sivakumar, 2015).

As is well known, silver (Ag) is a high electrically conductive metal with superior photocatalytic and antibacterial activity (Ma et al., 2020a; Panchal et al., 2020; Zhang et al., 2020a). Considering these features of silver, Zhang et al. (2016) developed a novel type of multifunctional MicroPCMs containing n-eicosane core and Ag/SiO_2 hybrid shell through interfacial polycondensation and silver reduction (Figure 17A). The resultant MicroPCMs have a perfect silver outer layer when the reaction time for reducing and depositing silver ions is set to 20 h. In addition to high LHS (155 J/g) and good thermal regulation capability, MicroPCMs have also a high electrical conductivity of 130 Ω·m. Therefore, the multifunctional MicroPCMs can be considered as conductive coatings to achieve anti-interference and cooling functions for central processing units and various memory chips. More importantly, MicroPCMs have high antimicrobial activities (Figures 17B–17F) against *Bacillus subtilis* (95.9%) and *Staphylococcus aureus* (99.1%) at a contact time of 4 h due to the perfect silver outer layer. Similarly, Wang et al. (2018a) also developed multifunctional MicroPCMs containing

n-octadecane core and Ag/SiO_2 hybrid shell (Figure 17G). The resultant MicroPCMs also exhibit excellent thermoregulation and bactericidal properties, especially for *Staphylococcus aureus*. Benefiting from good sterilization and thermal regulation functions, MicroPCMs can also satisfy the special requirement for the multifunctional surgical bandages that need both antibacterial and cooling effects on the wounds to promote their healing (Nischala et al., 2011).

In summary, MicroPCMs and NEPCMs with single SiO_2 shell usually exhibit relatively insufficient thermal performances and lack some advanced new functions., whereas MicroPCMs and NEPCMs with hybrid shells (SiO_2-organic hybrid shell and SiO_2-inorganic hybrid shell) can effectively solve the aforementioned shortcomings. They usually exhibit better thermal performances and many new functions (including electromagnetic shielding, electrochemical energy storage, and superhydrophobic, magnetic, fluorescent, photocatalytic, and antibacterial functions). To further satisfy special function requirements in some special application scenarios, MicroPCMs and NEPCMs with more advanced functions need to be further developed in the future.

CONCLUSIONS AND FUTURE PROSPECTS

This review provides state-of-the-art advances in SiO_2-based composite PCMs for thermal energy storage from the perspective of tailoring chemistry strategies. In this review, SiO_2-based composite PCMs are classified into porous shape-stabilized and micro/nano-encapsulated SiO_2-based composite PCMs according to the microstructures of SiO_2. In SiO_2-based composite PCMs, PCMs can complete heat storage and heat release by undergoing phase change, and SiO_2-based supporting materials can hinder the flow of liquid PCMs, thus maintaining solid state on a macroscopic scale. However, not all porous SiO_2 materials and SiO_2 microcapsules are suitable for the infiltration of PCMs. Because the physicochemical properties of SiO_2, including surface functional groups, pore sizes, dopants, single shell, and hybrid shells, inevitably influence the thermal performances and other functions of composite PCMs, including heat latent, phase change temperature, thermal conductivity, thermal stability, and shape stability. Especially, when SiO_2 is in the nanoscale, the resultant composite PCMs are much different from the bulk PCMs. Therefore, this review systematically summarizes and discusses the influences of surface functional groups, pore sizes, dopants, single shell, and hybrid shells on the thermal performances of SiO_2-based composite PCMs, aiming to provide in-depth insights into the relationships between structural designs and thermal properties and a better guide on the tailor-made construction of high-performance SiO_2-based composite PCMs.

In terms of porous SiO_2-based shape-stabilized composite PCMs, micropores generally stimulate stronger nanoconfinement effects on the thermophysical properties of PCMs in the molecular dynamics. The stronger nanoconfinement effects might significantly reduce the thermal energy storage density and latent heat of PCMs; even the latent heat is zero. However, relatively large macropores are usually insufficient to adsorb PCMs owing to the weak physical interactions between PCMs and macropores. Therefore, high thermal energy storage density is usually not available in the relatively large macropores. In addition, different surface functional groups of SiO_2 have significant effects on the thermal properties of composite PCMs. Suitable functional groups can significantly improve the thermal properties of SiO_2-based composite PCMs. On the contrary, unsuitable functional groups will reduce the thermal properties of SiO_2-based composite PCMs or even loss of thermal performances. In terms of micro/nano-encapsulated SiO_2-based composite PCMs, single SiO_2 shell is usually unable to satisfy some special functional requirements, whereas hybrid shells containing SiO_2 shell and organic shells or other inorganic shells with some specific functions can endure the enhanced thermal properties or novel functions of micro/nano-encapsulated SiO_2-based composite PCMs, such as electromagnetic shielding, electrochemical energy storage, and superhydrophobic, magnetic, fluorescent, photocatalytic, and antibacterial functions.

Although numerous significant advancements have been made in SiO_2-based composite PCMs, more efforts are still required to further regulate their thermophysical performances. Many promising aspects and challenges are worth further investigating and conquering on the development of high-performance SiO_2-based composite PCMs in the future. (1) Mutual matching relationships between functional group types of SiO_2 and different PCMs need further clarifications. (2) The mechanisms of the influences of different modified pores on the thermal properties of PCMs infiltrated in porous SiO_2 need more systematic explanations, including pores size, pore distribution, and pore shape. (3) Multi-scale investigation on thermal energy storage and thermal conductivity of SiO_2-based composite PCMs should be conducted based on theoretical, numerical, and experimental methods. (4) Thermal properties of porous SiO_2-based shape-stabilized

composite PCMs should be further improved. (5) High-performance micro/nano-encapsulated SiO_2-based composite PCMs with other hybrid shells should be further developed. (6) Current researches mainly focus on SiO_2-based organic composite PCMs. Therefore, SiO_2-based inorganic composite PCMs need more researches and the corresponding supercooling degree should be further reduced. (7) Sol-gel method is a common way to prepare SiO_2-based composite PCMs, but the cost of raw materials is high. In this regard, natural SiO_2 serving as the supporting material is a more economical way to obtain SiO_2-based composite PCMs, such as diatomite. Preparation efficiency and cost should be considered to satisfy the demands of industrial applications. (8) Multifunctional SiO_2-based composite PCMs should be designed and optimized to satisfy the specific application requirements, including mechanical, optical, electrical, magnetic, and biological properties, etc., which is a very promising research topic in the future.

ACKNOWLEDGMENTS

This work was financially supported by the Fundamental Research Funds for the Central Universities (No. 2019NTST29), National Natural Science Foundation of China (No. 51902025), and China Postdoctoral Science Foundation (No. 2020T130060 and 2019M660520).

AUTHOR CONTRIBUTIONS

Conceptualization: X.C.; Visualization: X.C., Z.T., and P.C.; Writing – Original Draft: X.C. and Z.T.; Writing – Review & Editing: X.C. and H.G.; Format and Copyright: Y.C., Z.T., and J.L.; Funding Acquisition: X.C.; Supervision: X.C.

REFERENCES

Aftab, W., Huang, X., Wu, W., Liang, Z., Mahmood, A., and Zou, R. (2018). Nanoconfined phase change materials for thermal energy applications. Energy Environ. Sci. *11*, 1392–1424.

Aftab, W., Mahmood, A., Guo, W., Yousaf, M., Tabassum, H., Huang, X., Liang, Z., Cao, A., and Zou, R. (2019). Polyurethane-based flexible and conductive phase change composites for energy conversion and storage. Energy Storage Mater *20*, 401–409.

Alehosseini, E., and Jafari, S.M. (2019). Micro/nano-encapsulated phase change materials (PCMs) as emerging materials for the food industry. Trends Food Sci. Technol. *91*, 116–128.

Atinafu, D.G., Dong, W., Wang, C., and Wang, G. (2018a). Synthesis of porous carbon from cotton using an Mg (OH) 2 template for form-stabilized phase change materials with high encapsulation capacity, transition enthalpy and reliability. J. Mater. Chem. A *6*, 8969–8977.

Atinafu, D.G., Dong, W., Wang, J., Huang, X., Wang, J., Gao, H., and Wang, G. (2018b). Synthesis and characterization of paraffin/metal organic gel derived porous carbon/boron nitride composite phase change materials for thermal energy storage. Eur. J. Inorg. Chem. *2018*, 5167–5175.

Bayat, M., Yang, H., Ko, F., Michelson, D., and Mei, A. (2014). Electromagnetic interference shielding effectiveness of hybrid multifunctional Fe_3O_4/carbon nanofiber composite. Poly *55*, 936–943.

Belessiotis, G.V., Papadokostaki, K.G., Favvas, E.P., Efthimiadou, E.K., and Karellas, S. (2018). Preparation and investigation of distinct and shape stable paraffin/SiO_2 composite PCM nanospheres. Energy Convers. Manage. *168*, 382–394.

Brown, E.N., Kessler, M.R., Sottos, N.R., and White, S.R. (2003). In situ poly (urea-formaldehyde) microencapsulation of dicyclopentadiene. J. Microencapsulation *20*, 719–730.

Cao, R., Wang, Y., Chen, S., Han, N., Liu, H., and Zhang, X. (2019). Multiresponsive shape-stabilized hexadecyl acrylate-grafted graphene as a phase change material with enhanced thermal and electrical conductivities. ACS Appl. Mater. Interfaces *11*, 8982–8991.

Chai, L., Wang, X., and Wu, D. (2015). Development of bifunctional microencapsulated phase change materials with crystalline titanium dioxide shell for latent-heat storage and photocatalytic effectiveness. Appl. Energy *138*, 661–674.

Chen, D., Chen, Y., Guo, X., Tao, W., Wang, J., Gao, S., and Gao, J. (2018a). Mesoporous silica nanoparticles with wrinkled structure as the matrix of myristic acid for the preparation of a promising new shape-stabilized phase change material via simple method. RSC Adv. *8*, 34224–34231.

Chen, X., Gao, H., Yang, M., Dong, W., Huang, X., Li, A., Dong, C., and Wang, G. (2018b). Highly graphitized 3D network carbon for shape-stabilized composite PCMs with superior thermal energy harvesting. Nano Energy *49*, 86–94.

Chen, D.-Z., Qin, S.-Y., Tsui, G.C., Tang, C.-y., Ouyang, X., Liu, J.-h., Tang, J.-N., and Zuo, J.-D. (2019a). Fabrication, morphology and thermal properties of octadecylamine-grafted graphene oxide-modified phase-change microcapsules for thermal energy storage. Compos. B Eng. *157*, 239–247.

Chen, D., Gao, H., Liu, P., Huang, P., and Huang, X. (2019b). Directly ambient pressure dried robust bridged silsesquioxane and methylsiloxane aerogels: effects of precursors and solvents. RSC Adv. *9*, 8664–8671.

Chen, X., Gao, H., Xing, L., Dong, W., Li, A., Cheng, P., Liu, P., and Wang, G. (2019c). Nanoconfinement effects of N-doped hierarchical carbon on thermal behaviors of organic phase change materials. Energy Storage Mater. *18*, 280–288.

Chen, X., Gao, H., Yang, M., Xing, L., Dong, W., Li, A., Zheng, H., and Wang, G. (2019d). Smart integration of carbon quantum dots in metal-organic frameworks for fluorescence-functionalized phase change materials. Energy Storage Mater. *18*, 349–355.

Chen, X., Gao, H., Hai, G., Jia, D., Xing, L., Chen, S., Cheng, P., Han, M., Dong, W., and Wang, G. (2020a). Carbon nanotube bundles assembled flexible hierarchical framework based phase change material composites for thermal energy harvesting and thermotherapy. Energy Storage Mater. *26*, 129–137.

Chen, X., Tang, Z., Gao, H., Chen, S., and Wang, G. (2020b). Phase change materials for electro-thermal conversion and storage: from fundamental understanding to engineering design. iScience *23*, 101208.

Chen, X., Tang, Z., Liu, P., Gao, H., Chang, Y., and Wang, G. (2020c). Smart utilization of multifunctional metal oxides in phase change materials. Matter *3*, 708–741.

Cho, J.-S., Kwon, A., and Cho, C.-G. (2002). Microencapsulation of octadecane as a phase-change material by interfacial polymerization in an emulsion system. Colloid Polym. Sci. *280*, 260–266.

Delgado, M., Lázaro, A., Mazo, J., and Zalba, B. (2012). Review on phase change material emulsions and microencapsulated phase change material slurries: materials, heat transfer studies and applications. Renew. Sustain. Energy Rev. *16*, 253–273.

Du, K., Calautit, J., Wang, Z., Wu, Y., and Liu, H. (2018). A review of the applications of phase change materials in cooling, heating and power generation in different temperature ranges. Appl. Energy *220*, 242–273.

Erdem, S., and Gürbüz, E. (2019). Influence of microencapsulated phase change materials on the flexural behavior and micromechanical impact damage of hybrid fibre reinforced engineered cementitious composites. Compos. B Eng. *166*, 633–644.

Fan, S., Gao, H., Dong, W., Tang, J., Wang, J., Yang, M., and Wang, G. (2017). Shape-stabilized phase change materials based on stearic acid and mesoporous hollow SiO_2 microspheres (SA/SiO_2) for thermal energy storage. Eur. J. Inorg. Chem. *2017*, 2138–2143.

Fang, G., Li, H., Chen, Z., and Liu, X. (2010). Preparation and characterization of flame retardant n-hexadecane/silicon dioxide composites as thermal energy storage materials. J. Hazard. Mater. *181*, 1004–1009.

Feng, L., Zhao, W., Zheng, J., Frisco, S., Song, P., and Li, X. (2011). The shape-stabilized phase change materials composed of polyethylene glycol and various mesoporous matrices (AC, SBA-15 and MCM-41). Sol. Energy Mater. Sol. Cells *95*, 3550–3556.

Feng, D., Feng, Y., Li, P., Zang, Y., Wang, C., and Zhang, X. (2020). Modified mesoporous silica filled with PEG as a shape-stabilized phase change materials for improved thermal energy storage performance. Microporous Mesoporous Mater. *292*, 109756.

Fredi, G., Dorigato, A., Fambri, L., and Pegoretti, A. (2017). Wax confinement with carbon nanotubes for phase changing epoxy blends. Polymers *9*, 405.

Fredi, G., Dorigato, A., Fambri, L., and Pegoretti, A. (2018). Multifunctional epoxy/carbon fiber laminates for thermal energy storage and release. Compos. Sci. Technol. *158*, 101–111.

Fredi, G., Dirè, S., Callone, E., Ceccato, R., Mondadori, F., and Pegoretti, A. (2019a). Docosane-organosilica microcapsules for structural composites with thermal energy storage/release capability. Materials *12*, 1286.

Fredi, G., Dorigato, A., Unterberger, S., Artuso, N., and Pegoretti, A. (2019b). Discontinuous carbon fiber/polyamide composites with microencapsulated paraffin for thermal energy storage. J. Appl. Polym. Sci. *136*, 47408.

Fu, W., Liang, X., Xie, H., Wang, S., Gao, X., Zhang, Z., and Fang, Y. (2017). Thermophysical properties of n-tetradecane@polystyrene-silica composite nanoencapsulated phase change material slurry for cold energy storage. Energy Build *136*, 26–32.

Fu, W., Zou, T., Liang, X., Wang, S., Gao, X., Zhang, Z., and Fang, Y. (2019). Preparation and properties of phase change temperature-tuned composite phase change material based on sodium acetate trihydrate–urea/fumed silica for radiant floor heating system. Appl. Therm. Eng. *162*, 114253.

Gao, H., Wang, J., Chen, X., Wang, G., Huang, X., Li, A., and Dong, W. (2018). Nanoconfinement effects on thermal properties of nanoporous shape-stabilized composite PCMs: a review. Nano Energy *53*, 769–797.

Gao, H., Bo, L., Liu, P., Chen, D., Li, A., Ou, Y., Dong, C., Wang, J., Chen, X., and Hou, C. (2019). Ambient pressure dried flexible silica aerogel for construction of monolithic shape-stabilized phase change materials. Sol. Energy Mater. Sol. Cells *201*, 110122.

Geisler, M., Netz, R.R., and Hugel, T. (2010). Pulling a single polymer molecule off a substrate reveals the binding thermodynamics of cosolutes. Angew. Chem. Int. Ed. *49*, 4730–4733.

Geng, L., Wang, S., Wang, T., and Luo, R. (2016). Facile synthesis and thermal properties of nanoencapsulated n-dodecanol with SiO_2 shell as shape-formed thermal energy storage material. Energy Fuels *30*, 6153–6160.

Giro-Paloma, J., Martínez, M., Cabeza, L.F., and Fernández, A.I. (2016). Types, methods, techniques, and applications for microencapsulated phase change materials (MPCM): a review. Renew. Sustain. Energy Rev. *53*, 1059–1075.

Grosu, Y., Zhao, Y., Giacomello, A., Meloni, S., Dauvergne, J.-L., Nikulin, A., Palomo, E., Ding, Y., and Faik, A. (2020). Hierarchical macro-nanoporous metals for leakage-freeygrosu@cicenergigune. com high-thermal conductivity shape-stabilized phase change materials. Appl. Energy *269*, 115088.

Gurav, J.L., Jung, I.-K., Park, H.-H., Kang, E.S., and Nadargi, D.Y. (2010). Silica aerogel: synthesis and applications. J. Nanomater. *2010*, 23.

He, F., Wang, X., and Wu, D. (2014). New approach for sol–gel synthesis of microencapsulated n-octadecane phase change material with silica wall using sodium silicate precursor. Energy *67*, 223–233.

He, F., Wang, X., and Wu, D. (2015). Phase-change characteristics and thermal performance of form-stable n-alkanes/silica composite phase change materials fabricated by sodium silicate precursor. Renew. Energy *74*, 689–698.

He, L., Mo, S., Lin, P., Jia, L., Chen, Y., and Cheng, Z. (2020). D-mannitol@silica/graphene oxide nanoencapsulated phase change material with high phase change properties and thermal reliability. Appl. Energy *268*, 115020.

Hou, D., Tao, H., Zhu, X., and Li, M. (2017). Polydopamine and MnO_2 core-shell composites for high-performance supercapacitors. Appl. Surf. Sci. *419*, 580–585.

Hu, H. (2020). Recent advances of polymeric phase change composites for flexible electronics and thermal energy storage system. Compos. B Eng. *195*, 108094.

Hu, Q., Li, J.J., Hao, Z.P., Li, L.D., and Qiao, S.Z. (2009). Dynamic adsorption of volatile organic compounds on organofunctionalized SBA-15 materials. Chem. Eng. J. *149*, 281–288.

Hu, N., Li, H., Wei, Q., Zhou, K., Zhu, W., Zhang, L., Li, S., Ye, W., Jiao, Z., and Luo, J. (2020). Continuous diamond-carbon nanotube foams as rapid heat conduction channels in composite phase change materials based on the stable hierarchical structure. Compos. B Eng. *200*, 108293.

Huang, X., Liu, Z., Xia, W., Zou, R., and Han, R.P. (2015). Alkylated phase change composites for thermal energy storage based on surface-modified silica aerogels. J. Mater. Chem. A *3*, 1935–1940.

Huang, Z., Luo, Z., Gao, X., Fang, X., Fang, Y., and Zhang, Z. (2017). Investigations on the thermal stability, long-term reliability of $LiNO_3$/KCl-expanded graphite composite as industrial waste heat storage material and its corrosion properties with metals. Appl. Energy *188*, 521–528.

Huang, X., Chen, X., Li, A., Atinafu, D., Gao, H., Dong, W., and Wang, G. (2019). Shape-stabilized phase change materials based on porous supports for thermal energy storage applications. Chem. Eng. J. *356*, 641–661.

Hussain, S., Ameelia Roseline, A., and Kalaiselvam, S. (2018). Bifunctional nanoencapsulated eutectic phase change material core with SiO_2/SnO_2 nanosphere shell for thermal and electrical energy storage. Mater. Des. *154*, 291–301.

Hyun, D.C., Levinson, N.S., Jeong, U., and Xia, Y. (2014). Emerging applications of phase-change materials (PCMs): teaching an old dog new tricks. Angew. Chem. Int. Ed. *53*, 3780–3795.

Ibrahim, N.I., Al-Sulaiman, F.A., Rahman, S., Yilbas, B.S., and Sahin, A.Z. (2017). Heat transfer enhancement of phase change materials for thermal energy storage applications: a critical review. Renew. Sustain. Energy Rev. *74*, 26–50.

Jamekhorshid, A., Sadrameli, S., and Farid, M. (2014). A review of microencapsulation methods of phase change materials (PCMs) as a thermal energy storage (TES) medium. Renew. Sustain. Energy Rev. *31*, 531–542.

Jiang, F., Wang, X., and Wu, D. (2014). Design and synthesis of magnetic microcapsules based on n-eicosane core and Fe_3O_4/SiO_2 hybrid shell for dual-functional phase change materials. Appl. Energy *134*, 456–468.

Jiang, F., Wang, X., and Wu, D. (2016). Magnetic microencapsulated phase change materials with an organo-silica shell: design, synthesis and application for electromagnetic shielding and thermal regulating polyimide films. Energy *98*, 225–239.

Jiang, Z., Ouyang, T., Yang, Y., Chen, L., Fan, X., Chen, Y., Li, W., and Fei, Y. (2018). Thermal conductivity enhancement of phase change materials with form-stable carbon bonded carbon fiber network. Mater. Des. *143*, 177–184.

Johari, G. (2009). Origin of the enthalpy features of water in 1.8 nm pores of MCM-41 and the large C p increase at 210 K. J. Chem. Phys. *130*, 124518.

Kadoono, T., and Ogura, M. (2014). Heat storage properties of organic phase-change materials confined in the nanospace of mesoporous SBA-15 and CMK-3. Phys. Chem. Chem. Phys. *16*, 5495–5498.

Kakar, M.R., Refaa, Z., Worlitschek, J., Stamatiou, A., Partl, M.N., and Bueno, M. (2019). Effects of aging on asphalt binders modified with

microencapsulated phase change material. Compos. B Eng. *173*, 107007.

Kaur, M., Umar, A., Mehta, S.K., and Kansal, S.K. (2019). Reduced graphene oxide-CdS heterostructure: an efficient fluorescent probe for the sensing of Ag (I) and sunset yellow and a visible-light responsive photocatalyst for the degradation of levofloxacin drug in aqueous phase. Appl. Catal. B: Environ. *245*, 143–158.

Kosmulski, M.J.J.o.C., and Science, I. (2002). The pH-dependent surface charging and the points of zero charge. J. Colloid Interface Sci. *253*, 77–87.

Li, B., Liu, T., Hu, L., Wang, Y., and Gao, L. (2013). Fabrication and properties of microencapsulated paraffin@SiO_2 phase change composite for thermal energy storage. ACS Sustain. Chem. Eng. *1*, 374–380.

Li, F., Wang, X., and Wu, D. (2015). Fabrication of multifunctional microcapsules containing n-eicosane core and zinc oxide shell for low-temperature energy storage, photocatalysis, and antibiosis. Energy Convers. Manage. *106*, 873–885.

Li, A., Dong, C., Dong, W., Atinafu, D.G., Gao, H., Chen, X., and Wang, G. (2018a). Hierarchical 3D reduced graphene porous-carbon-based PCMs for superior thermal energy storage performance. ACS Appl. Mater. Interfaces *10*, 32093–32101.

Li, G., Hong, G., Dong, D., Song, W., and Zhang, X. (2018b). Multiresponsive graphene-aerogel-directed phase-change smart fibers. Adv. Mater. *30*, 1801754.

Li, M., Liu, J., and Shi, J. (2018c). Synthesis and properties of phase change microcapsule with SiO_2-TiO_2 hybrid shell. Sol. Energy *167*, 158–164.

Li, C., Xie, B., Chen, J., He, Z., Chen, Z., and Long, Y. (2019). Emerging mineral-coupled composite phase change materials for thermal energy storage. Energy Convers. Manage. *183*, 633–644.

Li, B., Shu, D., Wang, R., Zhai, L., Chai, Y., Lan, Y., Cao, H., and Zou, C. (2020). Polyethylene glycol/silica (PEG@SiO_2) composite inspired by the synthesis of mesoporous materials as shape-stabilized phase change material for energy storage. Renew. Energy *145*, 84–92.

Liang, S., Li, Q., Zhu, Y., Chen, K., Tian, C., Wang, J., and Bai, R. (2015). Nanoencapsulation of n-octadecane phase change material with silica shell through interfacial hydrolysis and polycondensation in miniemulsion. Energy *93*, 1684–1692.

Lin, Y., Alva, G., and Fang, G. (2018a). Review on thermal performances and applications of thermal energy storage systems with inorganic phase change materials. Energy *165*, 685–708.

Lin, Y., Jia, Y., Alva, G., and Fang, G. (2018b). Review on thermal conductivity enhancement, thermal properties and applications of phase change materials in thermal energy storage. Renew. Sustain. Energy Rev. *82*, 2730–2742.

Lin, Y., Zhu, C., and Fang, G. (2019). Synthesis and properties of microencapsulated stearic acid/silica composites with graphene oxide for improving thermal conductivity as novel solar thermal storage materials. Sol. Energy Mater. Sol. Cells *189*, 197–205.

Liu, C., Rao, Z., Zhao, J., Huo, Y., and Li, Y. (2015). Review on nanoencapsulated phase change materials: preparation, characterization and heat transfer enhancement. Nano Energy *13*, 814–826.

Liu, J., Wang, Q., Ling, Z., Fang, X., and Zhang, Z. (2017a). A novel process for preparing molten salt/expanded graphite composite phase change blocks with good uniformity and small volume expansion. Sol. Energy Mater. Sol. Cells *169*, 280–286.

Liu, S., Yan, Z., Fu, L., and Yang, H. (2017b). Hierarchical nano-activated silica nanosheets for thermal energy storage. Sol. Energy Mater. Sol. Cells *167*, 140–149.

Liu, H., Wang, X., and Wu, D. (2018a). Tailoring of bifunctional microencapsulated phase change materials with CdS/SiO_2 double-layered shell for solar photocatalysis and solar thermal energy storage. Appl. Therm. Eng. *134*, 603–614.

Liu, Z., Wei, H., Tang, B., Xu, S., and Shufen, Z. (2018b). Novel light-driven CF/PEG/SiO_2 composite phase change materials with high thermal conductivity. Sol. Energy Mater. Sol. Cells *174*, 538–544.

Liu, H., Niu, J., Wang, X., and Wu, D. (2019a). Design and construction of mesoporous silica/n-eicosane phase-change nanocomposites for supercooling depression and heat transfer enhancement. Energy *188*, 116075.

Liu, H., Wang, X., Wu, D., and Ji, S. (2019b). Fabrication and applications of dual-responsive microencapsulated phase change material with enhanced solar energy-storage and solar photocatalytic effectiveness. Sol. Energy Mater. Sol. Cells *193*, 184–197.

Liu, Z., Chen, Z., and Yu, F. (2019c). Preparation and characterization of microencapsulated phase change materials containing inorganic hydrated salt with silica shell for thermal energy storage. Sol. Energy Mater. Sol. Cells *200*, 110004.

Liu, P., Gao, H., Chen, X., Chen, D., Lv, J., Han, M., Cheng, P., and Wang, G. (2020). In situ one-step construction of monolithic silica aerogel-based composite phase change materials for thermal protection. Compos. B Eng. *195*, 108072.

Lu, X., Huang, H., Zhang, X., Lin, P., Huang, J., Sheng, X., Zhang, L., and Qu, J.-p. (2019). Novel light-driven and electro-driven polyethylene glycol/two-dimensional MXene form-stable phase change material with enhanced thermal conductivity and electrical conductivity for thermal energy storage. Compos. B Eng. *177*, 107372.

Luan, Y., Yang, M., Ma, Q., Qi, Y., Gao, H., Wu, Z., and Wang, G. (2016). Introduction of an organic acid phase changing material into metal–organic frameworks and the study of its thermal properties. J. Mater. Chem. A *4*, 7641–7649.

Lv, Y., Liu, G., Zhang, G., and Yang, X. (2020a). A novel thermal management structure using serpentine phase change material coupled with forced air convection for cylindrical battery modules. J. Power Sources *468*, 228398.

Lv, Y., Yang, X., and Zhang, G. (2020b). Durability of phase-change-material module and its relieving effect on battery deterioration during long-term cycles. Appl. Therm. Eng. *179*, 115747.

Lyu, J., Liu, Z., Wu, X., Li, G., Fang, D., and Zhang, X. (2019). Nanofibrous Kevlar aerogel films and their phase-change composites for highly efficient infrared stealth. ACS Nano *13*, 2236–2245.

Ma, X., Liu, Y., Liu, H., Zhang, L., Xu, B., and Xiao, F. (2018). Fabrication of novel slurry containing graphene oxide-modified microencapsulated phase change material for direct absorption solar collector. Sol. Energy Mater. Sol. Cells *188*, 73–80.

Ma, Y., Xie, Q., and Wang, X. (2019). Investigations on thermal properties of microencapsulated phase-change materials with different acrylate-based copolymer shells as thermal insulation materials. J. Appl. Polym. Sci. *136*, 47777.

Ma, C., Yang, Z., Wang, W., Zhang, M., Hao, X., Zhu, S., and Chen, S. (2020a). Fabrication of Ag-Cu_2O/PANI nanocomposites for visible-light photocatalysis triggering super antibacterial activity. J. Mater. Chem. C *8*, 2888–2898.

Ma, Y., Hai, G., Atinafu, D.G., Dong, W., Li, R., Hou, C., and Wang, G. (2020b). Carbon inserted defect-rich MoS_2-X nanosheets@CdS nanospheres for efficient photocatalytic hydrogen evolution under visible light irradiation. J. Colloid Interface Sci. *569*, 89–100.

Manoj Kumar, P., Mylsamy, K., and Saravanakumar, P.T. (2020). Experimental investigations on thermal properties of nano-SiO_2/paraffin phase change material (PCM) for solar thermal energy storage applications. Energy Sources Part A *42*, 2420–2433.

Matei, C., Buhălțeanu, L., Berger, D., and Mitran, R.-A. (2019). Functionalized mesoporous silica as matrix for shape-stabilized phase change materials. Int. J. Heat Mass Transfer *144*, 118699.

Milian, Y.E., Gutierrez, A., Grageda, M., and Ushak, S. (2017). A review on encapsulation techniques for inorganic phase change materials and the influence on their thermophysical properties. Renew. Sustain. Energy Rev. *73*, 983–999.

Min, X., Fang, M., Huang, Z., Liu, Y.g., Huang, Y., Wen, R., Qian, T., and Wu, X. (2015). Enhanced thermal properties of novel shape-stabilized PEG composite phase change materials with radial mesoporous silica sphere for thermal energy storage. Sci. Rep. *5*, 12964.

Mitran, R.A., Berger, D., Munteanu, C., and Matei, C. (2015). Evaluation of different mesoporous silica supports for energy storage in shape-stabilized phase change materials with dual thermal responses. J. Phys. Chem. C *119*, 15177–15184.

Mohamed, S.A., Al-Sulaiman, F.A., Ibrahim, N.I., Zahir, M.H., Al-Ahmed, A., Saidur, R., Yılbaş, B., and Sahin, A. (2017). A review on current status and challenges of inorganic phase change materials for thermal energy storage systems. Renew. Sustain. Energy Rev. *70*, 1072–1089.

Munaiah, Y., Raj, B.G.S., Kumar, T.P., and Ragupathy, P. (2013). Facile synthesis of hollow sphere amorphous MnO 2: the formation mechanism, morphology and effect of a bivalent cation-containing electrolyte on its supercapacitive behavior. J. Mater. Chem. A *1*, 4300–4306.

Nadargi, D.Y., Kalesh, R.R., and Rao, A.V. (2009). Rapid reduction in gelation time and impregnation of hydrophobic property in the tetraethoxysilane (TEOS) based silica aerogels using NH4F catalyzed single step sol-gel process. J. Alloys Compd. *480*, 689–695.

Neill, S.P., Angeloudis, A., Robins, P.E., Walkington, I., Ward, S.L., Masters, I., Lewis, M.J., Piano, M., Avdis, A., and Piggott, M.D. (2018). Tidal range energy resource and optimization–Past perspectives and future challenges. Renew. Energy *127*, 763–778.

Nischala, K., Rao, T.N., and Hebalkar, N. (2011). Silica-silver core-shell particles for antibacterial textile application. Colloids Surf. B. *82*, 203–208.

Nomura, T., Zhu, C., Sheng, N., Tabuchi, K., Sagara, A., and Akiyama, T. (2015). Shape-stabilized phase change composite by impregnation of octadecane into mesoporous SiO_2. Sol. Energy Mater. Sol. Cells *143*, 424–429.

Panchal, P., Paul, D.R., Sharma, A., Choudhary, P., Meena, P., and Nehra, S. (2020). Biogenic mediated Ag/ZnO nanocomposites for photocatalytic and antibacterial activities towards disinfection of water. J. Colloid Interface Sci. *563*, 370–380.

Pardo, P., Deydier, A., Anxionnaz-Minvielle, Z., Rougé, S., Cabassud, M., and Cognet, P. (2014). A review on high temperature thermochemical heat energy storage. Renew. Sustain. Energy Rev. *32*, 591–610.

Pethurajan, V., Sivan, S., Konatt, A.J., and Reddy, A.S. (2018). Facile approach to improve solar thermal energy storage efficiency using encapsulated sugar alcohol based phase change material. Sol. Energy Mater. Sol. Cells *185*, 524–535.

Pielichowska, K., and Pielichowski, K. (2014). Phase change materials for thermal energy storage. Prog. Mater Sci. *65*, 67–123.

Qian, T., Li, J., Ma, H., and Yang, J. (2015a). The preparation of a green shape-stabilized composite phase change material of polyethylene glycol/SiO_2 with enhanced thermal performance based on oil shale ash via temperature-assisted sol-gel method. Sol. Energy Mater. Sol. Cells *132*, 29–39.

Qian, T., Li, J., Min, X., Guan, W., Deng, Y., and Ning, L. (2015b). Enhanced thermal conductivity of PEG/diatomite shape-stabilized phase change materials with Ag nanoparticles for thermal energy storage. J. Mater. Chem. A *3*, 8526–8536.

Qian, T., Li, J., Min, X., Deng, Y., Guan, W., and Ning, L. (2016). Radial-like mesoporous silica sphere: a promising new candidate of supporting material for storage of low-, middle-, and high-temperature heat. Energy *112*, 1074–1083.

Qian, T., Li, J., Min, X., and Fan, B. (2017). Integration of pore confinement and hydrogen-bond influence on the crystallization behavior of C18 PCMs in mesoporous silica for form-stable phase change materials. ACS Sustain. Chem. Eng. *6*, 897–908.

Qian, T., Zhu, S., Wang, H., Li, A., and Fan, B. (2018). Comparative study of single-walled carbon nanotubes and graphene nanoplatelets for improving the thermal conductivity and solar-to-light conversion of PEG-infiltrated phase-change material composites. ACS Sustain. Chem. Eng. *7*, 2446–2458.

Qian, T., Dang, B., Chen, Y., Jin, C., Qian, J., and Sun, Q. (2019). Fabrication of magnetic phase change n-eicosane@Fe_3O_4/SiO_2 microcapsules on wood surface via sol-gel method. J. Alloys Compd. *772*, 871–876.

Qiu, X., Lu, L., Wang, J., Tang, G., and Song, G. (2015). Fabrication, thermal properties and thermal stabilities of microencapsulated n-alkane with poly (lauryl methacrylate) as shell. Thermochim. Acta *620*, 10–17.

Qu, Y., Chen, J., Liu, L., Xu, T., Wu, H., and Zhou, X. (2020). Study on properties of phase change foam concrete block mixed with paraffin/fumed silica composite phase change material. Renew. Energy *150*, 1127–1135.

Qureshi, Z.A., Ali, H.M., and Khushnood, S. (2018). Recent advances on thermal conductivity enhancement of phase change materials for energy storage system: a review. Int. J. Heat Mass Transfer *127*, 838–856.

Ranjbar, S.G., Roudini, G., and Barahuie, F. (2020). Fabrication and characterization of phase change material-SiO2 nanocomposite for thermal energy storage in buildings. J. Energy Storage *27*, 101168.

Rudner, M.S., Jeremic, S., Petterson, K.A., Kent IV, D.R., Brown, K.A., Drake, M.D., Goddard, W.A., and Roberts, J.D. (2005). Intramolecular hydrogen bonding in disubstituted ethanes. a comparison of NH…O- and OH…O- hydrogen bonding through conformational analysis of 4-amino-4-oxobutanoate (succinamate) and monohydrogen 1, 4-butanoate (monohydrogen succinate) anions. J. Phys. Chem. A *109*, 9076–9082.

Saffari, M., de Gracia, A., Fernández, C., Belusko, M., Boer, D., and Cabeza, L.F. (2018). Optimized demand side management (DSM) of peak electricity demand by coupling low temperature thermal energy storage (TES) and solar PV. Appl. Energy *211*, 604–616.

Şahan, N., and Paksoy, H. (2018). Novel shapeable phase change material (PCM) composites for thermal energy storage (TES) applications. Sol. Energy Mater. Sol. Cells *174*, 380–387.

Sánchez, L., Sánchez, P., de Lucas, A., Carmona, M., and Rodríguez, J.F. (2007). Microencapsulation of PCMs with a polystyrene shell. Colloid Polym. Sci. *285*, 1377–1385.

Sarı, A., and Biçer, A. (2012). Thermal energy storage properties and thermal reliability of some fatty acid esters/building material composites as novel form-stable PCMs. Sol. Energy Mater. Sol. Cells *101*, 114–122.

Saxena, R., Rakshit, D., and Kaushik, S. (2019). Phase change material (PCM) incorporated bricks for energy conservation in composite climate: a sustainable building solution. Sol. Energy *183*, 276–284.

Sharma, R., Ganesan, P., Tyagi, V., Metselaar, H., and Sandaran, S. (2015). Developments in organic solid–liquid phase change materials and their applications in thermal energy storage. Energy Convers. Manage. *95*, 193–228.

Shchukina, E., Graham, M., Zheng, Z., and Shchukin, D. (2018). Nanoencapsulation of phase change materials for advanced thermal energy storage systems. Chem. Soc. Rev. *47*, 4156–4175.

Shen, J., Zhang, P., Song, L., Li, J., Ji, B., Li, J., and Chen, L. (2019). Polyethylene glycol supported by phosphorylated polyvinyl alcohol/graphene aerogel as a high thermal stability phase change material. Compos. B Eng. *179*, 107545.

Shi, Y., and Zhou, B. (2019). Melamine foam impregnated with paraffin as thermal regulation materials for obtaining stable indoor temperature. Energy Build *183*, 650–658.

Shi, L., He, Y., Hu, Y., and Wang, X. (2018). Thermophysical properties of Fe_3O_4@CNT nanofluid and controllable heat transfer performance under magnetic field. Energy Convers. Manage. *177*, 249–257.

Shin, H.K., Rhee, K.-Y., and Park, S.-J. (2016). Effects of exfoliated graphite on the thermal properties of erythritol-based composites used as phase-change materials. Compos. B Eng. *96*, 350–353.

Song, S., Zhao, T., Zhu, W., Qiu, F., Wang, Y., and Dong, L. (2019). Natural microtubule-encapsulated phase-change material with simultaneously high latent-heat capacity and enhanced thermal conductivity. ACS Appl. Mater. Interfaces *11*, 20828–20837.

Su, J., Wang, L., and Ren, L. (2006). Fabrication and thermal properties of microPCMs: used melamine-formaldehyde resin as shell material. J. Appl. Polym. Sci. *101*, 1522–1528.

Sudha, D., and Sivakumar, P. (2015). Review on the photocatalytic activity of various composite catalysts. Chem. Eng. Process. *97*, 112–133.

Sun, J., Zhang, Q., Guo, F., Gu, J., and Zhang, J. (2012). Preparation and characterization of magnetic polyimide hybrid thin films. J. Appl. Polym. Sci. *125*, 725–730.

Sun, H., Xu, Z., and Gao, C. (2013). Multifunctional, ultra-flyweight, synergistically assembled carbon aerogels. Adv. Mater. *25*, 2554–2560.

Sun, K., Liu, H., Wang, X., and Wu, D. (2019). Innovative design of superhydrophobic thermal energy-storage materials by microencapsulation of n-docosane with nanostructured ZnO/SiO_2 shell. Appl. Energy *237*, 549–565.

Taguchi, Y., Yokoyama, H., Kado, H., and Tanaka, M. (2007). Preparation of PCM microcapsules by using oil absorbable polymer particles. Colloids Surf. A *301*, 41–47.

Tang, X., Luo, L., Guo, Y., Yang, Z., Zhang, K., He, R., Fan, J., and Yang, W. (2019). Preparation and light-to-heat conversion efficiency of paraffin/graphene aerogel shape-stable phase change materials. Fuller. Nanotubes Carbon Nanostruct. *27*, 375–381.

Tang, B., Qiu, M., and Zhang, S. (2012). Thermal conductivity enhancement of PEG/SiO_2 composite PCM by in situ Cu doping. Sol. Energy Mater. Sol. Cells *105*, 242–248.

Tang, B., Wang, Y., Qiu, M., and Zhang, S. (2014a). A full-band sunlight-driven carbon nanotube/

PEG/SiO2 composites for solar energy storage. Sol. Energy Mater. Sol. Cells *123*, 7–12.

Tang, B., Wu, C., Qiu, M., Zhang, X., and Zhang, S. (2014b). PEG/SiO_2-Al_2O_3 hybrid form-stable phase change materials with enhanced thermal conductivity. Mater. Chem. Phys. *144*, 162–167.

Tang, B., Wei, H., Zhao, D., and Zhang, S. (2017). Light-heat conversion and thermal conductivity enhancement of PEG/SiO_2 composite PCM by in situ Ti_4O_7 doping. Sol. Energy Mater. Sol. Cells *161*, 183–189.

Tang, J., Chen, X., Zhang, L., Yang, M., Wang, P., Dong, W., Wang, G., Yu, F., and Tao, J. (2018). Alkylated meso-macroporous metal-organic framework hollow tubes as nanocontainers of octadecane for energy storage and thermal regulation. Small *14*, 1801970.

Tong, X., Li, N., Zeng, M., and Wang, Q. (2019). Organic phase change materials confined in carbon-based materials for thermal properties enhancement: recent advancement and challenges. Renew. Sustain. Energy Rev. *108*, 398–422.

Tu, J., Li, H., Cai, Z., Zhang, J., Hu, X., Huang, J., Xiong, C., Jiang, M., and Huang, L. (2019). Phase change-induced tunable dielectric permittivity of poly (vinylidene fluoride)/polyethylene glycol/graphene oxide composites. Compos. B Eng. *173*, 106920.

Umair, M.M., Zhang, Y., Iqbal, K., Zhang, S., and Tang, B. (2019). Novel strategies and supporting materials applied to shape-stabilize organic phase change materials for thermal energy storage-A review. Appl. Energy *235*, 846–873.

Wang, W., Yang, X., Fang, Y., Ding, J., and Yan, J. (2009). Enhanced thermal conductivity and thermal performance of form-stable composite phase change materials by using β-Aluminum nitride. Appl. Energy *86*, 1196–1200.

Wang, C., Feng, L., Li, W., Zheng, J., Tian, W., and Li, X. (2012). Shape-stabilized phase change materials based on polyethylene glycol/porous carbon composite: the influence of the pore structure of the carbon materials. Sol. Energy Mater. Sol. Cells *105*, 21–26.

Wang, W., Gumfekar, S.P., Jiao, Q., and Zhao, B. (2013). Ferrite-grafted polyaniline nanofibers as electromagnetic shielding materials. J. Mater. Chem. C *1*, 2851–2859.

Wang, L.P., Li, Q.F., Wang, C., and Lan, X.Z. (2014a). Size-dependent phase behavior of the hexadecane–octadecane system confined in nanoporous glass. J. Phys. Chem. C *118*, 18177–18186.

Wang, W., Zang, C., and Jiao, Q. (2014b). Synthesis, structure and electromagnetic properties of Mn-Zn ferrite by sol–gel combustion technique. J. Magn. Magn. Mater. *349*, 116–120.

Wang, L.P., Sui, J., Zhai, M., Tian, F., and Lan, X.Z. (2015). Physical control of phase behavior of hexadecane in nanopores. J. Phys. Chem. C *119*, 18697–18706.

Wang, H., Luo, J., Yang, Y., Zhao, L., Song, G., and Tang, G. (2016a). Fabrication and characterization of microcapsulated phase change materials with an additional function of thermochromic performance. Solar Energy *139*, 591–598.

Wang, J., Yang, M., Lu, Y., Jin, Z., Tan, L., Gao, H., Fan, S., Dong, W., and Wang, G. (2016b). Surface functionalization engineering driven crystallization behavior of polyethylene glycol confined in mesoporous silica for shape-stabilized phase change materials. Nano Energy *19*, 78–87.

Wang, H., Li, Y., Zhao, L., Shi, X., Song, G., and Tang, G. (2018a). A facile approach to synthesize microencapsulated phase change materials embedded with silver nanoparicle for both thermal energy storage and antimicrobial purpose. Energy *158*, 1052–1059.

Wang, H., Zhao, L., Song, G., Tang, G., and Shi, X. (2018b). Organic-inorganic hybrid shell microencapsulated phase change materials prepared from SiO_2/TiC-stabilized pickering emulsion polymerization. Sol. Energy Mater. Sol. Cells *175*, 102–110.

Wang, S., Zhu, B., Liu, M., Zhang, L., Yu, J., and Zhou, M. (2019a). Direct Z-scheme ZnO/CdS hierarchical photocatalyst for enhanced photocatalytic H_2-production activity. Appl. Catal. B: Environ. *243*, 19–26.

Wang, W., Umair, M.M., Qiu, J., Fan, X., Cui, Z., Yao, Y., and Tang, B. (2019b). Electromagnetic and solar energy conversion and storage based on Fe3O4-functionalised graphene/phase change material nanocomposites. Energy Convers. Manage. *196*, 1299–1305.

Wu, S., Li, T., Tong, Z., Chao, J., Zhai, T., Xu, J., Yan, T., Wu, M., Xu, Z., and Bao, H. (2019). High-performance thermally conductive phase change composites by large-size oriented graphite sheets for scalable thermal energy harvesting. Adv. Mater. *31*, 1905099.

Wu, Y., and Wang, T. (2015). The dependence of phase change enthalpy on the pore structure and interfacial groups in hydrated salts/silica composites via sol-gel. J. Colloid Interface Sci. *448*, 100–105.

Wu, C.-B., Wu, G., Yang, X., Liu, Y.-J., Gao, C.-X., Ji, Q.-H., Wang, M., and Chen, H.-Z. (2014). Preparation of Mannitol@Silica core-shell capsules via an interfacial polymerization process from water-in-oil emulsion. Colloids Surf. A *457*, 487–494.

Wu, C.-B., Wu, G., Yang, X., Liu, Y.-J., Liang, T., Fu, W.-F., Wang, M., and Chen, H.-Z. (2015). Preparation of microencapsulated medium temperature phase change material of Tris (hydroxymethyl) methyl aminomethane@SiO_2 with excellent cycling performance. Appl. Energy *154*, 361–368.

Wu, X., Ding, J., Kong, Y., Sun, Z., Shao, G., Li, B., Wu, J., Zhong, Y., Shen, X., and Cui, S. (2018). Synthesis of a novel three-dimensional Na_2SO_4@SiO_2@Al_2O_3-SiO_2 phase change material doped aerogel composite with high thermal resistance and latent heat. Ceram. Int. *44*, 21855–21865.

Wu, S., Yan, T., Kuai, Z., and Pan, W. (2020). Thermal conductivity enhancement on phase change materials for thermal energy storage: a review. Energy Storage Mater. *25*, 251–295.

Xia, Y., Cui, W., Ji, R., Huang, C., Huang, Y., Zhang, H., Xu, F., Huang, P., Li, B., and Sun, L. (2020). Design and synthesis of novel microencapsulated phase change materials with enhancement of thermal conductivity and thermal stability: self-assembled boron nitride into shell materials. Colloids Surf. A *586*, 124225.

Xiangfa, Z., Hanning, X., Jian, F., Changrui, Z., and Yonggang, J. (2012). Preparation, properties and thermal control applications of silica aerogel infiltrated with solid-liquid phase change materials. J. Exp. Nanosci. *7*, 17–26.

Xiao, C., Zhang, G., Li, Z., and Yang, X. (2020). Custom design of solid-solid phase change material with ultra-high thermal stability for battery thermal management. J. Mater. Chem. A *8*, 14624–14633.

Xu, Y., and Schoonen, M.A. (2000). The absolute energy positions of conduction and valence bands of selected semiconducting minerals. Am. Mineral. *85*, 543–556.

Xu, Q., Liu, H., Wang, X., and Wu, D. (2018). Smart design and construction of nanoflake-like MnO2/SiO2 hierarchical microcapsules containing phase change material for in-situ thermal management of supercapacitors. Energy Convers. Manage. *164*, 311–328.

Xue, F., Lu, Y., Qi, X.-d., Yang, J.-h., and Wang, Y. (2019). Melamine foam-templated graphene nanoplatelet framework toward phase change materials with multiple energy conversion abilities. Chem. Eng. J. *365*, 20–29.

Yang, S., Song, X., Zhang, P., and Gao, L. (2013). Facile synthesis of nitrogen-doped graphene–ultrathin MnO_2 sheet composites and their electrochemical performances. ACS Appl. Mater. Interfaces *5*, 3317–3322.

Yang, G., Yim, Y.J., Lee, J.W., Heo, Y.J., and Park, S.J. (2019a). Carbon-filled organic phase-change materials for thermal energy storage: a review. Molecules *24*, 2055.

Yang, J., Tang, L.-S., Bai, L., Bao, R.-Y., Liu, Z.-Y., Xie, B.-H., Yang, M.-B., and Yang, W. (2019b). High-performance composite phase change materials for energy conversion based on macroscopically three-dimensional structural materials. Mater. Horiz. *6*, 250–273.

Yang, W., Feng, Y., Si, Q., Yan, Q., Long, P., Dong, L., Fu, L., and Feng, W. (2019c). Efficient cycling utilization of solar-thermal energy for thermochromic displays with controllable heat output. J. Mater. Chem. A *7*, 97–106.

Yang, Z., Mao, Z., Xiang, B., and Zhang, J. (2019d). Construction of a binary channel efficient cooling composites with reflective and phase-change properties. Compos. B Eng. *178*, 107517.

Yu, Q., Jiang, Z., Cong, L., Lu, T., Suleiman, B., Leng, G., Wu, Z., Ding, Y., and Li, Y. (2019). A novel low-temperature fabrication approach of composite phase change materials for high temperature thermal energy storage. Appl. Energy *237*, 367–377.

Yuan, K., Shi, J., Aftab, W., Qin, M., Usman, A., Zhou, F., Lv, Y., Gao, S., and Zou, R. (2020). Engineering the thermal conductivity of functional phase-change materials for heat

energy conversion, storage, and utilization. Adv. Funct. Mater. *30*, 1904228.

Yun, S., Luo, H., and Gao, Y. (2014). Ambient-pressure drying synthesis of large resorcinol–formaldehyde-reinforced silica aerogels with enhanced mechanical strength and superhydrophobicity. J. Mater. Chem. A *2*, 14542–14549.

Zahir, M.H., Mohamed, S.A., Saidur, R., and Al-Sulaiman, F.A. (2019). Supercooling of phase-change materials and the techniques used to mitigate the phenomenon. Appl. Energy *240*, 793–817.

Zhang, Q., and Liu, J. (2019). Anisotropic thermal conductivity and photodriven phase change composite based on rt100 infiltrated carbon nanotube array. Sol. Energy Mater. Sol. Cells *190*, 1–5.

Zhang, D., Tian, S., and Xiao, D. (2007). Experimental study on the phase change behavior of phase change material confined in pores. Solar Energy *81*, 653–660.

Zhang, H., Sun, S., Wang, X., and Wu, D. (2011). Fabrication of microencapsulated phase change materials based on n-octadecane core and silica shell through interfacial polycondensation. Colloids Surf. A *389*, 104–117.

Zhang, L., Shi, H., Li, W., Han, X., and Zhang, X. (2013). Structure and thermal performance of poly (ethylene glycol) alkyl ether (Brij)/porous silica (MCM-41) composites as shape-stabilized phase change materials. Thermochim. Acta *570*, 1–7.

Zhang, Y.X., Huang, M., Li, F., Wang, X.L., and Wen, Z.Q. (2014). One-pot synthesis of hierarchical MnO_2-modified diatomites for electrochemical capacitor electrodes. J. Power Sources *246*, 449–456.

Zhang, Y., Wang, X., and Wu, D. (2015). Design and fabrication of dual-functional microcapsules containing phase change material core and zirconium oxide shell with fluorescent characteristics. Sol. Energy Mater. Sol. Cells *133*, 56–68.

Zhang, X., Wang, X., and Wu, D. (2016). Design and synthesis of multifunctional microencapsulated phase change materials with silver/silica double-layered shell for thermal energy storage, electrical conduction and antimicrobial effectiveness. Energy *111*, 498–512.

Zhang, Y., Li, X., Li, J., Ma, C., Guo, L., and Meng, X. (2018a). Solar-driven phase change microencapsulation with efficient Ti_4O_7 nanoconverter for latent heat storage. Nano Energy *53*, 579–586.

Zhang, Y., Zheng, S., Zhu, S., Ma, J., Sun, Z., and Farid, M. (2018b). Evaluation of paraffin infiltrated in various porous silica matrices as shape-stabilized phase change materials for thermal energy storage. Energy Convers. Manage. *171*, 361–370.

Zhang, L., An, L., Wang, Y., Lee, A., Schuman, Y., Ural, A., Fleischer, A.S., and Feng, G. (2019a). Thermal enhancement and shape stabilization of a phase-change energy-storage material via copper nanowire aerogel. Chem. Eng. J. *373*, 857–869.

Zhang, L., Zhou, K., Wei, Q., Ma, L., Ye, W., Li, H., Zhou, B., Yu, Z., Lin, C.-T., and Luo, J. (2019b). Thermal conductivity enhancement of phase change materials with 3D porous diamond foam for thermal energy storage. Appl. Energy *233*, 208–219.

Zhang, Y., Umair, M.M., Zhang, S., and Tang, B. (2019c). Phase change materials for electron-triggered energy conversion and storage: a review. J. Mater. Chem. A *7*, 22218–22228.

Zhang, Y., Wang, J., Qiu, J., Jin, X., Umair, M.M., Lu, R., Zhang, S., and Tang, B. (2019d). Ag-graphene/PEG composite phase change materials for enhancing solar-thermal energy conversion and storage capacity. Appl. Energy *237*, 83–90.

Zhang, Y., Zhang, J., Li, X., and Wu, X. (2019e). Preparation of hydrophobic lauric acid/SiO_2 shape-stabilized phase change materials for thermal energy storage. J. Energy Storage *21*, 611–617.

Zhang, C., Gu, Y., Teng, G., Wang, L., Jin, X., Qiang, Z., and Ma, W. (2020a). Designation of double-shell Ag/AgCl/G-$ZnFe_2O_4$ nanocube with enhanced light absorption and superior photocatalytic antibacterial activity. ACS Appl. Mater. Interfaces *12*, 29883–29898.

Zhang, X., Lin, Q., Luo, H., and Luo, S. (2020b). Three-dimensional graphitic hierarchical porous carbon/stearic acid composite as shape-stabilized phase change material for thermal energy storage. Appl. Energy *260*, 114278.

Zhao, C.-Y., and Zhang, G.H. (2011). Review on microencapsulated phase change materials (MEPCMs): fabrication, characterization and applications. Renew. Sustain. Energy Rev. *15*, 3813–3832.

Zhen, W., Ning, X., Yang, B., Wu, Y., Li, Z., and Lu, G. (2018). The enhancement of CdS photocatalytic activity for water splitting via anti-photocorrosion by coating Ni_2P shell and removing nascent formed oxygen with artificial gill. Appl. Catal. B: Environ. *221*, 243–257.

Zhu, Y., Liang, S., Chen, K., Gao, X., Chang, P., Tian, C., Wang, J., and Huang, Y. (2015). Preparation and properties of nanoencapsulated n-octadecane phase change material with organosilica shell for thermal energy storage. Energy Convers. Manage. *105*, 908–917.

Zhu, Y., Liang, S., Wang, H., Zhang, K., Jia, X., Tian, C., Zhou, Y., and Wang, J. (2016). Morphological control and thermal properties of nanoencapsulated n-octadecane phase change material with organosilica shell materials. Energy Convers. Manage. *119*, 151–162.

Zhu, Y., Qin, Y., Wei, C., Liang, S., Luo, X., Wang, J., and Zhang, L. (2018). Nanoencapsulated phase change materials with polymer-SiO_2 hybrid shell materials: compositions, morphologies, and properties. Energy Convers. Manage. *164*, 83–92.

Zhu, Y., Qin, Y., Liang, S., Chen, K., Tian, C., Wang, J., Luo, X., and Zhang, L. (2019). Graphene/SiO_2/n-octadecane nanoencapsulated phase change material with flower like morphology, high thermal conductivity, and suppressed supercooling. Appl. Energy *250*, 98–108.